metals

MDPI

Review

A Review of Metastable Beta Titanium Alloys

R. Prakash Kolli [1,*] and Arun Devaraj [2]

[1] Department of Materials Science and Engineering, University of Maryland, College Park, MD 20742, USA
[2] Physical and Computational Sciences Directorate, Pacific Northwest National Laboratory, Richland, WA 99354, USA; arun.devaraj@pnnl.gov
* Correspondence: pkolli@umd.edu; Tel.: +1-301-405-5217; Fax: 301-405-6327

Received: 21 May 2018; Accepted: 25 June 2018; Published: 30 June 2018

Abstract: In this article, we provide a broad and extensive review of beta titanium alloys. Beta titanium alloys are an important class of alloys that have found use in demanding applications such as aircraft structures and engines, and orthopedic and orthodontic implants. Their high strength, good corrosion resistance, excellent biocompatibility, and ease of fabrication provide significant advantages compared to other high performance alloys. The body-centered cubic (bcc) β-phase is metastable at temperatures below the beta transus temperature, providing these alloys with a wide range of microstructures and mechanical properties through processing and heat treatment. One attribute important for biomedical applications is the ability to adjust the modulus of elasticity through alloying and altering phase volume fractions. Furthermore, since these alloys are metastable, they experience stress-induced transformations in response to deformation. The attributes of these alloys make them the subject of many recent studies. In addition, researchers are pursuing development of new metastable and near-beta Ti alloys for advanced applications. In this article, we review several important topics of these alloys including phase stability, development history, thermo-mechanical processing and heat treatment, and stress-induced transformations. In addition, we address recent developments in new alloys, phase stability, superelasticity, and additive manufacturing.

Keywords: beta phase; metastable; titanium; aircraft; biomedical; superelasticity; additive manufacturing

1. Introduction

Titanium and its alloys are commercially important for many industries [1,2]. They are used for engineering applications in the aerospace industry [1,3–5], the biomedical and healthcare industry [1,5–13], the energy and power generation industry [1,5,14,15], and the petrochemical industry [5]. For example, commercially pure (cp) α-titanium (α-Ti) is used in the biomedical industry as an orthodontic or orthopedic implant material due to its good biocompatibility, excellent corrosion resistance, and low cytotoxicity. In another application, the Ti-6Al-4V (wt. %) alloy, which is a dual-phase $\alpha + \beta$ alloy, is used extensively in the aerospace industry due to its high specific strength, σ/ρ, and high specific stiffness, E/ρ, which leads to weight reduction and space savings. In a third illustration, the Ti-13V-13Cr-3Al (wt. %) alloy was the first successfully developed and commercialized β-phase Ti alloy. It was used extensively in the SR-71 "Blackbird" aircraft because of its high specific strength leading to weight savings and also its stable elevated temperature properties.

The major disadvantage of titanium alloys is the high cost, which is due in part to raw material costs and but largely due to extraction and processing costs [1,4]. The use of titanium in engineering applications has, however, experienced persistent growth due to its mechanical response and physical behavior advantages [4]. In the case of commercial aircraft, titanium alloys accounted for a small

fraction of the total structural and engine weight when first introduced. The quantity of titanium in structures and engines has increased dramatically in the latest generations of commercial aircraft approaching ~9% of the total weight in Boeing 777 aircraft and ~15% of the total weight in Boeing 787 aircraft [1,4]. A recent industry report highlighted that the annual growth rate for titanium demand in aircraft structures grew at ~14% between 2011 and 2016 [16]. In general, titanium alloys are used in high value applications where the trade off between improved performance and the higher costs of the alloys are justified.

The utility and broad range of mechanical and physical properties for titanium alloys is due primarily to its allotropy in the sold-state. There are two crystallographic allotropes, which are the hexagonal close-packed (hcp) α-phase and the higher-temperature body-centered cubic (bcc) β-phase. Controlled alloying and thermo-mechanical processing can create titanium alloy variations based on microstructural and compositional differences, which in turn allows modifying the mechanical and physical properties of the alloys tailored towards a specific application. In general, there are three broad classifications of room temperature titanium alloys, which are the alpha phase alloys, the dual-phase α + β alloys, and the beta phase alloys [1,3,17]. The alpha phase Ti alloys predominantly contain primary hcp α-phase but may contain smaller quantities of other phases. They are generally used in non-structural applications where low strength and good corrosion resistance are required [1]. These alloys often contain aluminum (Al) and small quantities of interstitial elements such oxygen (O), nitrogen (N), and carbon (C) in order to stabilize the hcp α-phase [18]. Higher strength versions contain a greater quantity of O that acts to increase the yield strength and tensile strength but reduce ductility of alpha phase Ti alloys [19,20]. Dual-phase α + β Ti alloys contain a mixture of both phases and are generally used in applications requiring higher strength, good toughness, good fatigue behavior, and excellent corrosion resistance [1]. The phase morphology and relative volume fraction of each phase depends on the composition of the alloy and thermo-mechanical processing. The combination of higher strengths, a density of 4.5 g/cm^3, and phase stability give this class of alloys excellent specific properties that extend to high temperatures of about 600 °C (1112 °F). The most well known of this class of alloys is Ti-6Al-4V (wt. %) but also include alloys such as Ti-6Al-6V-2Sn (wt. %), and Ti-6Al-2Sn-4Zr-6Mo (wt. %). These alloys often contain Al as an alpha phase stabilizing element but also contain beta phase stabilizing elements such as vanadium (V) or molybdenum (Mo). Solution treatment and age hardening are often used to control the final microstructure. Additional information about both of these classes of alloys can be found in recent review articles and texts [1,5]. The third type of Ti alloys is the beta phase alloy, which can be further sub-divided into near-beta Ti alloys, metastable beta Ti alloys, and the stable beta Ti alloys. A fourth category is the beta matrix (or beta-rich) α + β dual-phase Ti alloy that we include in the broad classification of beta phase alloys although it may also be included as a dual-phase α + β Ti alloy. Metastable β-phase alloys, which is the focus of this article, consists predominantly of the bcc β-phase but can also contain small volume fractions of martensitic phases or the athermal ω-phase depending on composition and thermo-mechanical processing [1]. These alloys will also contain secondary hcp α-phase platelets or particles formed during isothermal aging. Metastable β-phase alloys are used in structural applications where high specific strengths, low elastic modulus, good fatigue resistance, sufficient toughness, excellent corrosion resistance, and good formability are required. Metastable β-phase Ti alloys also possess excellent biocompatibility leading to their use in implants. This class of alloys contains sufficient quantities of beta phase stabilizing elements in order to ensure that close to 100 vol. % of metastable bcc β-phase is retained at room temperature after quenching from the single-phase field. The characteristics of metastable β-phase Ti alloys make them an attractive choice for advanced engineering applications in demanding conditions despite their high costs [1]. Notwithstanding their promise, these alloys have mainly seen use in niche applications for aircraft structures, orthopedic implants, and orthodontic devices. For instance, the metastable Ti-3Al-8V-6Cr-4Mo-4Zr (wt. %) alloy, also known as Beta C, is used in aircraft springs and fasteners [21]. In a second example, the metastable Ti-29Nb-13Ta-4.6Zr (wt. %) alloy was developed for implants based partially on its excellent biocompatibility [22]. The near-beta Ti alloy commercially known as

"TMA" (titanium-molybdenum alloy) with a nominal composition of Ti-11.5Mo-6Zr-4.5Sn (wt. %) was developed for use in orthodontic wires [23]. Recently there has been renewed interest in this important class of Ti alloys as exemplified by current research for aircraft structures and engines and biomedical applications [24–32].

Past review articles of metastable β-phase Ti alloys have addressed classification [17], phase stability [33], heat treatment [34], and application in aircraft structures [21,35,36]. Other review articles of metastable β-phase Ti alloys have focused on mechanical properties and biocompatibility in biomedical implants [6–9,11,13]. The objective of this review article is to provide a broad and extensive review of developments in this class of alloys, which has not been addressed in the literature. This article discusses current state of research on commercially important alloys for aerospace structures and biomedical implants in context of alloy design, processing and heat treatment, and phase transformations. We provide an update of the state of current research in several important topics and address areas that are being actively researched. We first discuss in detail beta phase stabilizing elements, alpha phase stabilizing elements, and neutral elements and their influence on the bcc β-phase stability. The latest research and limitations about understanding the effects of O and Zr on the metastable ω-phase and martensitic phases is discussed. In the third section, we provide an overview of the development history of metastable beta titanium alloys in aircraft structures and biomedical orthopedic implants. Current important and newly developed alloys are discussed. Requirements for further development towards new applications are also considered. In this section we also briefly examine future trends of these alloys. In the fourth section we address Ti alloy production, thermo-mechanical processing, and heat treatment of these alloys. In the fifth section we discuss stress-induced transformations, which are an inherent characteristic of these alloys. In the last section, we also discuss recent research on processing of beta Ti alloys by metal additive manufacturing (AM). The review is concluded by summarizing and discussing challenges for expanded application of metastable β-phase Ti alloys and design of new alloys. In the summary section, challenges and future directions for fundamental scientific research are considered. Specifically, we address experimental and computational techniques that can facilitate greater understanding of these alloys and further their development.

2. Alloying Elements and Molybdenum Equivalency

2.1. Beta Phase Stabilizing Elements

In general, metastable beta phase Ti alloys are designed and heat-treated so that they retain close to 100 vol. % of the bcc β-phase when quenched from the single β-phase field to room temperature. This is accomplished by alloying with sufficient quantities of beta phase stabilizing elements to suppress the formation of the hcp α'-martensite phase, the orthorhombic α''-martensite phase, and the equilibrium hcp α-phase during quenching. Most of these stabilizing elements are transition metals and are classified as one of two types, either isomorphous or eutectoid, depending on the effect of alloying on Ti, Table 1. Certain binary phase diagrams do not exhibit a miscibility gap when alloyed with some isomorphous elements, such as niobium (Nb) and tantalum (Ta). The equilibrium phase diagram does not display invariant reactions, congruent transformations, or critical points. On the other hand, some binary phase diagrams exhibit a monotectoid reaction when alloyed with other isomorphous elements, such as molybdenum (Mo), vanadium (V), and tungsten (W). This difference is illustrated between a Ti-Nb phase diagram [37] in Figure 1a and Ti-Mo phase diagram [37] in Figure 1b. The second type of beta phase stabilizing elements is denoted eutectoid elements. These elements are not miscible in Ti exhibiting limited solid solubility, and form an eutectoid point and reaction $\beta \leftrightarrow \alpha + \mathrm{Ti}_x\mathrm{A}_y$, where $\mathrm{Ti}_x\mathrm{A}_y$ is an intermetallic compound of the Ti and an eutectoid alloying element A. Eutectoid elements include iron (Fe), chromium (Cr), copper (Cu), nickel (Ni), cobalt (Co), manganese (Mn), and silicon (Si). Hydrogen (H) is also classified in the category of eutectoid alloying elements. This type of reaction is illustrated for a Ti-Cr phase diagram [37,38] in Figure 1c.

The eutectoid point in the phase diagram is observed at an approximately 14 wt. % Cr concentration and an isotherm of 667 °C (1233 °F). The intermetallic compound that is formed is the Laves α-$TiCr_2$ phase. In general, the isomorphous and eutectoid elements lower the beta transus temperature, T_β, which is the lowest temperature that 100 vol. % of the bcc β-phase will exist, increase the size of the single β-phase field, decrease the size of the hcp α-phase field, or deliver a combination of these three effects, Figure 2. The effect on the Ti alloy microstructure by alloying with a beta phase stabilizing element depends on the concentration. If the beta phase stabilizing element is included only in a limited quantity that is less than the critical concentration listed in Table 1, then the Ti alloy microstructure will consist of only the hcp α-phase after quenching from above the quantity T_β, such as in the binary Ti-1.6 wt. % V alloy [39,40]. Although the beta phase stabilizing element V is included in the binary alloy, the concentration is significantly less than the critical concentration of 15 wt. % required to stabilize the bcc β-phase. If greater quantities of beta phase stabilizing elements are included, then the Ti alloy will have a dual-phase $\alpha + \beta$ alloy microstructure after quenching from above the beta transus temperature, such as in the binary Ti-8.1 wt. % V alloy [41–43]. However, an alloy will generally consist of only the metastable bcc β-phase after quenching from above the beta transus temperature when the V concentration is greater than the critical quantity needed to stabilize the bcc β-phase [44]. It is theoretically possible to add sufficient quantities of stabilizing elements to lower the quantity T_β below room temperature resulting in a stable beta phase Ti alloy. In this case, since the bcc β-phase is stable, it does not undergo phase decomposition during aging and is thus not hardenable, unlike the metastable beta phase Ti alloys. The quantity of beta phase stabilizing elements required to result in a stable alloy is greater than the critical concentrations listed in Table 1 for binary Ti alloys and is schematically depicted in Figure 2.

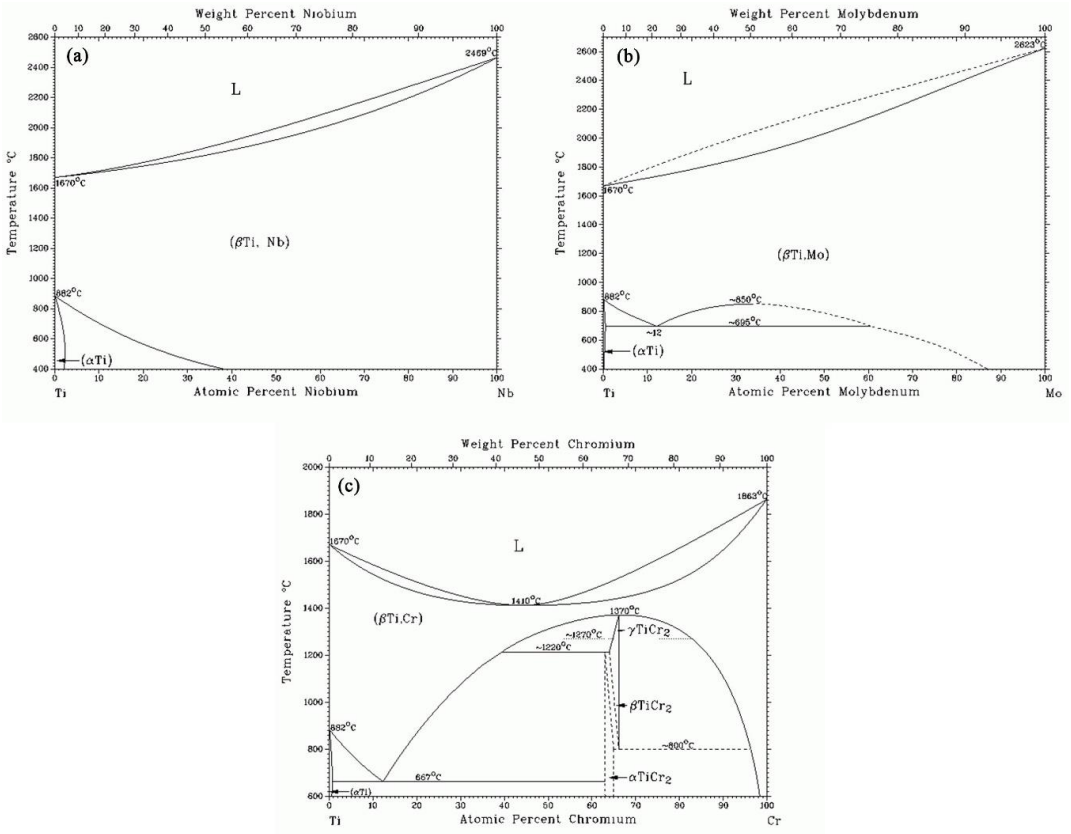

Figure 1. Example titanium binary phase diagrams illustrating an isomorphous phase diagram with no miscibility gap in (**a**) Ti-Nb, an isomorphous phase diagram with a monotectoid reaction in (**b**) Ti-Mo, and an eutectoid phase diagram in (**c**) Ti-Cr [37,38].

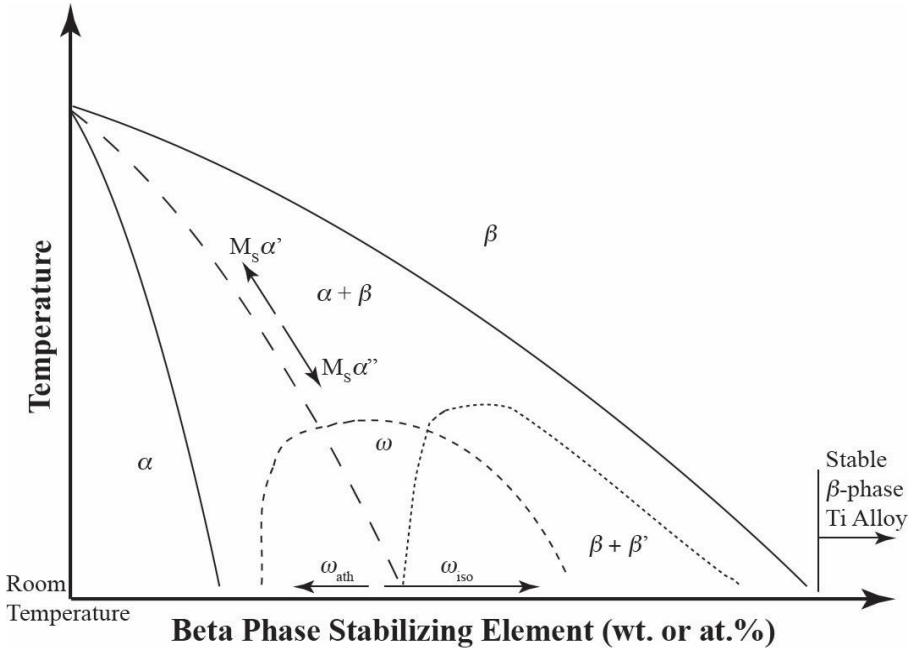

Figure 2. A schematic of a pseudo-binary isomorphous phase diagram. The schematic illustrates the metastable hcp α'-martensite start temperature $M_{S\alpha'}$, orthorhombic α''-martensite start temperature $M_{S\alpha''}$, metastable ω-phase field, and metastable bcc β-phase field. The equilibrium hcp α-phase field is also depicted. The beta phase stabilizing element concentration differences between the hexagonal (or trigonal) athermal ω-phase (ω_{ath}) and hexagonal isothermal ω-phase (ω_{iso}) are shown.

Table 1. Critical concentrations (wt. %) of beta phase stabilizing elements in binary Ti alloys required to retain 100% of the bcc β-phase after quenching to room temperature.

Element	Isomorphous or Eutectoid	Critical Concentration (wt. %)
Molybdenum	Isomorphous	10.0
Niobium	Isomorphous	36.0
Tantalum	Isomorphous	45.0
Vanadium	Isomorphous	15.0
Tungsten	Isomorphous	22.5
Cobalt	Eutectoid	7.0
Copper	Eutectoid	13.0
Chromium	Eutectoid	6.5
Iron	Eutectoid	3.5
Manganese	Eutectoid	6.5
Nickel	Eutectoid	9.0

Whether the hcp α'-martensite phase and the orthorhombic α''-martensite phase are suppressed during quenching depends on the quantity of beta phase stabilizing elements in the alloy. At concentrations below the critical concentration, the metastable martensitic phases will form. For example, the α'-martensite phase forms at Mo concentrations between 1 and 4 wt. % but at concentrations between 4 and 10 wt. % Mo the α''-martensite phase forms in a binary Ti-Mo alloy [45]. At Mo concentrations greater than 10 wt. %, the martensitic transformations are completely suppressed as a result of quenching from above the quantity T_β, forming only the metastable bcc β-phase [45]. The morphology of the martensitic phases was observed to change from massive (lamellar colonies) to acicular with increasing Mo concentration. A comparable result was observed in the binary Ti-V alloy [46].

Besides the aforementioned phases, the metastable athermal ω-phase (ω_{ath}) is often observed in the microstructure of many commercial beta Ti alloys. This phase may form during quenching from the

single β-phase field to room temperature with a hexagonal (not close-packed) crystallographic structure at smaller concentrations of beta phase stabilizing elements (solute lean), whereas the crystallographic structure is trigonal at greater concentrations of beta phase stabilizing elements (solute rich) [34,47–50]. Furthermore, if present the metastable martensitic phases and athermal ω-phase will decompose during isothermal aging into $\alpha + \beta$, $\alpha + \beta + \omega_{iso}$, or $\beta + \omega_{iso}$ phases depending on the alloy's phase stability, aging temperature, and aging time. The hexagonal isothermal ω-phase (ω_{iso}) forms from the bcc β-phase as a result of low-temperature aging [21,34,49]. On the other hand, the bcc β-phase may undergo phase decomposition into $\beta + \beta'$ phases during aging in alloys containing quantities of beta phase stabilizing elements greater than the minimum concentrations listed in Table 1 and if the isothermal ω-phase is suppressed [34,49].

2.2. Alpha Phase Stabilizing Elements

Alpha phase stabilizing elements are often included as alloying elements in metastable β-phase Ti alloys. For example, 3 wt. % Al is added to the Ti-10V-2Fe-3Al (wt. %) alloy used in aircraft structures and landing gears. Elements such as Al increase the size of the hcp α-phase field or raise the temperature that the α–phase is stable. Contrary to expectations, these elements are added to promote beta phase stability [1]. The isothermal ω-phase increases the strength but reduces the ductility of Ti alloys and hence this phase is not desired in large quantities since it causes severe embrittlement [47,50,51]. Several early studies have illustrated that the addition of Al in binary Ti-V or Ti-Mo alloys reduces the isothermal ω-phase volume fraction and also limits the temporal stability of the ω-phase by accelerating the kinetics of the α-phase nucleation [34,49,51]. Additionally, the temperature at which the isothermal ω-phase forms was lowered preventing its formation at higher aging temperatures. Aluminum also decreases the start temperature, Ms, for martensitic transformations, which suppresses these phase transformations during quenching from the single β-phase field.

Other alpha phase stabilizing elements include interstitial O and N, which are extremely strong alpha phase stabilizing elements with high solid solubility [37,52–54]. Interstitial C is also an alpha phase stabilizing element but with lower solubility [1,52]. Similar to Al, these three interstitial elements increase the quantity T_β but are added to metastable β-phase Ti alloys since they suppress the formation of the embrittling isothermal ω-phase. In the case of O, which is often included in Ti alloys, it reduces the volume fraction of the hexagonal isothermal ω-phase that forms and hinders its kinetics of phase transformation relative to the hcp α-phase during aging [34,49]. Recently, two studies have suggested that O also suppresses formation of the orthorhombic α''-martensite phase during quenching by increasing the threshold stress for the transformation to occur [55,56]. These studies have also determined that the threshold stress increases with increasing O concentration. These results have significance for room temperature superelastic properties exhibited by some beta Ti alloys and are the subject of numerous research efforts.

2.3. Neutral Elements

Neutral elements, such as zirconium (Zr) and tin (Sn), do not significantly affect the quantity T_β. These elements are added to metastable beta phase Ti alloys because they are thought to alter the kinetics of hexagonal isothermal ω-phase formation during aging, which in turn stabilizes the bcc β-phase [1,34]. An important study by Williams et al., demonstrated that the addition of Zr or Sn to binary Ti-V alloys reduced the volume fraction of the isothermal ω-phase and in high enough concentrations suppressed its nucleation [53]. Similar results were observed in the same study for only Zr in binary Ti-Mo alloys. Zirconium and Sn may also decrease the Ms temperature [1], which suppresses the martensitic transformations. More recent results by Pang et al. [57] have, however, called into question the effect of Zr on suppressing the isothermal ω-phase formation during aging. In the study by Pang et al. [57], Zr additions up to 8 at. % in a model binary Ti-24Nb (at. %) alloy had little effect on the formation of the isothermal ω-phase following low-temperature aging at 300 °C

for 100 h. Since these new results contradict earlier studies, the effect of Zr on the stability of the isothermal ω-phase requires further study due to the importance of limiting embrittlement in current and new beta Ti alloys.

2.4. Molybdenum Equivalency (MoE)

For a given Ti alloy composition, a well-known and useful parameter for characterizing the β-phase stability is the molybdenum equivalency (MoE). This quantity is a combined measure of the effects of beta phase stabilizing elements, alpha phase stabilizing elements, and neutral elements contained in a Ti alloy on the beta phase stability. It uses Mo as an arbitrarily chosen baseline and normalizes other elements to an equivalent molybdenum value. The equation is given by [17,21,36,58]:

$$\begin{array}{l} \text{MoE} = 1.0(\text{wt.\% Mo}) + 0.67(\text{wt.\% V}) + 0.44(\text{wt.\% W}) \\ +0.28(\text{wt.\% Nb}) + 0.22(\text{wt.\% Ta}) + 2.9(\text{wt.\% Fe}) \\ +1.6(\text{wt.\% Cr}) + 1.25(\text{wt.\% Ni}) + 1.70(\text{wt.\% Mn}) \\ +1.70(\text{wt.\% Co}) - 1.0(\text{wt.\% Al}) \end{array} \quad (1)$$

The constant before each element concentration (in wt. %) in Equation (1) is the ratio of the critical concentration of Mo to retain 100 vol. % of the metastable bcc β-phase after quenching to room temperature and prevent formation of the martensitic phases to the critical concentration of the element needed to retain 100 vol. % of the metastable bcc β-phase after quenching to room temperature and prevent formation of the martensitic phases. The critical concentration for each beta phase stabilizing element is given in Table 1. Aluminum is subtracted because it is an alpha phase stabilizing element. The effect of the alpha phase stabilizing elements and the two neutral elements, Zr and Sn, are included in Equation (1) through the aluminum equivalency (AlE) given by [21]:

$$\begin{array}{l} \text{AlE} = 1.0(\text{wt.\% Al}) + 0.17(\text{wt.\% Zr}) \\ +0.33(\text{wt.\% Sn}) + 10(\text{wt.\% O} + \text{wt.\% N}) \end{array} \quad (2)$$

Minor variations in the coefficients and terms of Equations (1) and (2) have been published by Bania [36], Cotton et al. [21], and Welsch et al. [17]. These differences can partially be traced to differences in the critical concentrations of an element between U.S. and Russian data [34]. Equation (1) and Table 1 indicate that some beta phase stabilizing elements have a greater stabilizing effect than others. In general, a MoE value of approximately 10.0 is required to stabilize the bcc β-phase during quenching from above the beta transus temperature. The quantity T_β generally decreases with increasing MoE value, Figure 3. A high MoE value means that the alloy is heavily stabilized, which is typical of some current commercial alloys, such as Alloy C. The quantity MoE is thus a convenient metric to rank order the beta phase stability of not only model binary alloys but also commercial alloys. The MoE values of some model binary and commercially important beta Ti alloys is provided in Table 2. The classification of the four categories of beta Ti alloys is discussed below. A graphical representation of rank ordered MoE values for the beta Ti alloys in Table 2 is illustrated in Figure 4.

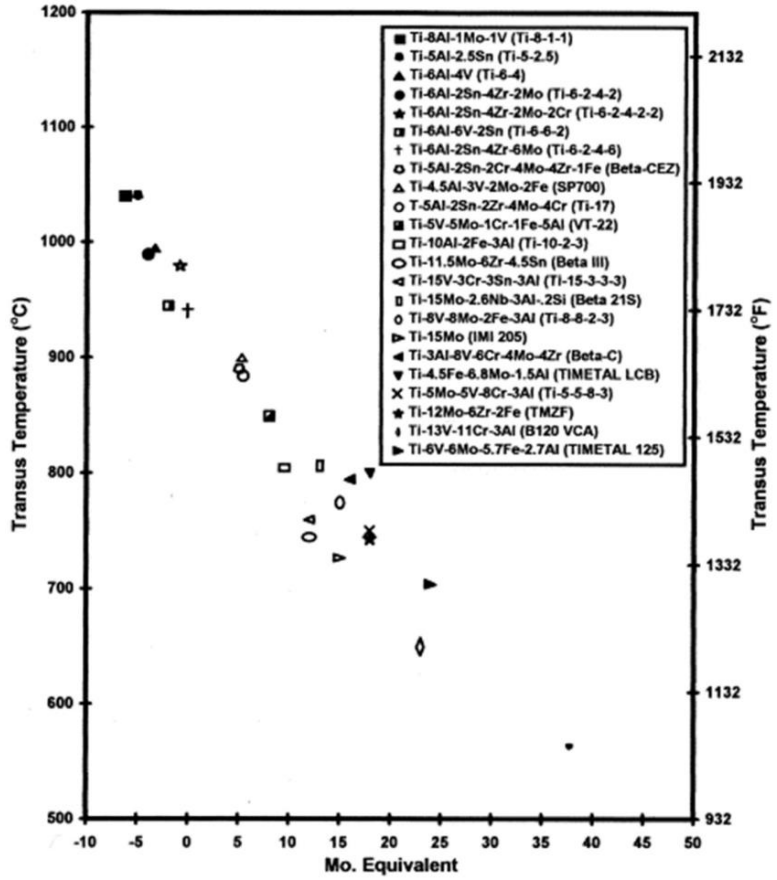

Figure 3. The beta transus temperature, T_β, plot as a function of molybdenum equivalency (MoE) for select alloys. The quantity T_β exhibits a generally decreasing trend with increasing MoE value [58]. (Reprinted by permission from Materials Science and Engineering A, vol. 243, no. 1–2, I. Weiss and S. L. Semiatin, Thermomechanical processing of beta titanium Alloys—an overview, 46–65, 1998, with permission from Elsevier).

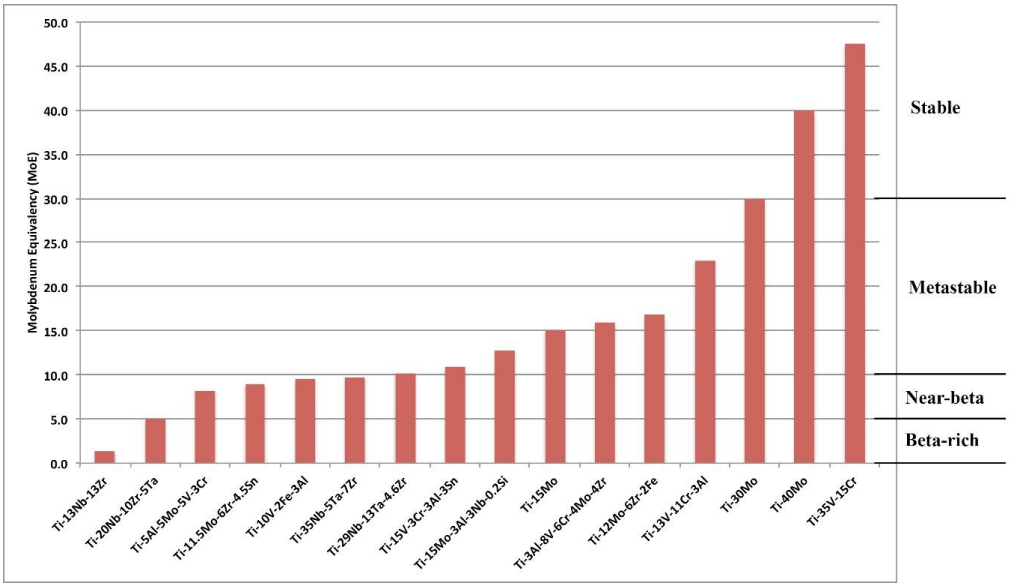

Figure 4. A plot of molybdenum equivalency (MoE) of model binary and commercially important beta Ti alloys listed in Table 2. Alloys with $0 \leq$ MoE < 5 are beta-rich, alloys with $5 \leq$ MoE < 10 are near-beta, alloys with $10 \leq$ MoE < 30 are metastable, and alloys with MoE > 30 are denoted stable.

Table 2. The molybdenum equivalency (MoE) and beta transus temperatures (T_β) of several model binary and commercially important beta Ti alloys. Compositions of the alloys are given in wt. %.

Alloy	Name	Application	Type	MoE	Beta Transus (°C)
Ti-13Nb-13Zr	-	Biomedical	Beta-rich	1.4	735
Ti-20Nb-10Zr-5Ta	TNZT	Biomedical	Near-Beta	5.0	-
Ti-5Al-5Mo-5V-3Cr	Ti-5553	Aircraft	Near-Beta	8.2	855–870
Ti-11.5Mo-6Zr-4.5Sn	TMA	Biomedical	Near-Beta	9.0	-
Ti-10V-2Fe-3Al	Ti-10-2-3	Aircraft	Near-Beta	9.5	790–805
Ti-35Nb-5Ta-7Zr	-	Biomedical	Near-Beta	9.7	-
Ti-29Nb-13Ta-4.6Zr	-	Biomedical	Metastable	10.2	-
Ti-15V-3Cr-3Al-3Sn	-	Aircraft	Metastable	10.9	750–770
Ti-15Mo-3Al-3Nb-0.2Si	Beta 21S	Aircraft	Metastable	12.8	795–810
Ti-15Mo	-	Model Binary	Metastable	15.0	-
Ti-3Al-8V-6Cr-4Mo-4Zr	Beta C	Aircraft/Oilfields	Metastable	16.0	715–740
Ti-12Mo-6Zr-2Fe	-	Biomedical	Metastable	16.8	-
Ti-13V-11Cr-3Al	B120 VCA	Aircraft	Metastable	23.0	650
Ti-30Mo	-	Model Binary	Stable	30.0	-
Ti-40Mo	-	Model Binary	Stable	40.0	-
Ti-35V-15Cr	Alloy C	Aircraft	Stable	47.5	unknown

An alternative parameter to describe a transition metal's alloying effect on the bcc β-phase stability in Ti is the elastic shear modulus, $C' = (C_{11} - C_{12})/2$ [17]. The quantity C' varies with the electron-to-atom (e/a) ratio, which is the ratio of valence electrons to atoms [59]. In context of the beta phase stabilizing elements that are transition metals the quantity (e/a) ranges in value between four to a maximum of approximately six [17]. The quantity C' becomes very small at an (e/a) value of four, which corresponds to the threshold for the martensitic transformations, and reaches a maximum at an (e/a) value of six. Within this range, an increase in the quantity C' corresponds to greater bcc β-phase stability in Ti [17].

2.5. Classification

In general, beta phase Ti alloys can be classified into four categories that are based approximately on the range of bcc β-phase stability and the MoE scale [21,58,60]. These categories are typically termed the beta matrix $\alpha + \beta$ (beta-rich) Ti alloy, near-beta Ti alloy, metastable beta Ti alloy, and the stable beta Ti alloy. The division between the three lower categories is somewhat subjective. Cotton et al. [21] have indicated that beta matrix $\alpha + \beta$ Ti alloys have a MoE < ~5.0, whereas near-beta Ti alloys have ~5.0 $\leq$ MoE $\leq$ ~10.0. The beta matrix $\alpha + \beta$ alloys possess a β-phase matrix with stable primary α-phase particles. An example is the Ti-5Al-2Sn-2Cr-4Mo-4Zr-1Fe (wt. %) alloy, which is referred to as Beta CEZ [61], and has a MoE value of 5.1. Since beta-matrix Ti alloys commonly have low MoE values the quantity for T_β is not lowered by a significant amount and it is approximately 890 °C (1634 °F) in Beta CEZ. In the context of the aforesaid definition, near-beta Ti alloys have slightly higher MoE values but can still be considered metastable beta Ti alloys and their composition places them near the $\alpha + \beta$ phase field and β-phase field boundaries. These alloys will usually have a β-phase matrix with stable primary α-phase grains and also secondary α-phase particles that form during aging. An example is the Ti-5553 alloy, which has a MoE value of 9.6 and the quantity T_β is approximately 865 °C (1589 °F) [21]. The MoE value for metastable beta Ti alloys are between ~10.0 and ~30.0 and near 100 vol. % of the bcc β-phase is typically retained during quenching. Since these alloys are metastable they can be heat-treated to increase the strength by aging and are deeply hardenable. The metastable Ti-3Al-8V-6Cr-4Mo-4Zr (wt. %) alloy, also known as Beta C, has a MoE value of 16.0 and the quantity T_β is approximately 730 °C (1346 °F). On the other hand, stable beta Ti alloys have a MoE > ~30.0, and are not hardenable since theoretically precipitation does not occur during aging [21,58]. The stable Ti-35V-15Cr (wt. %) alloy, also known as Alloy C, has a very high MoE value of 47.5.

3. Development History and Future Trends of Metastable Beta Titanium Alloys

3.1. Aircraft Structures

The development history of metastable beta Ti alloys can be traced to the early 1950's [36,58]. Bania mentions that patents were issued for corrosion-resistant Ti-30Mo (wt. %) to Ti-40Mo (wt. %) alloys at this time [36]. But these model binary alloys are considered stable beta Ti alloys due to their high concentration of beta stabilizing elements and high MoE values. However, these early efforts led to the development of metastable beta Ti alloys. The most successful early commercial metastable beta Ti alloy is Ti-13V-l1Cr-3Al (wt. %), which is referred to as B120 VCA and was developed by Crucible Steel Corporation in the early- to mid-1950's [35,36,58,62]. This alloy is well-known for its application in the structure and landing gear of the SR-71 "BlackBird" aircraft [21,35,36,58,62]. Boyer and Briggs indicate that approximately 93% of the aircraft was fabricated from Ti alloys and the majority was B120 VCA. One unique attribute of the B120 VCA alloy is that it is heat treatable but the alloy also possesses good thermal stability due to its MoE value of 23.0 that places it at the higher end of the metastable category. This allowed the alloy to be hot-worked, cold-worked, and aged to higher strengths. In addition, the good thermal stability permitted solution-treated sheets to be spot welded and used without aging at elevated temperatures such as in the SR-71 aircraft, which flew at Mach 3+ and saw in-service temperatures of approximately 288 °C (550 °F) [36]. The B120 VCA alloy's high specific strength also led to its use as springs in aircraft actuation systems [21]. Other early efforts to create metastable beta Ti alloys resulted in the Ti-1Al-8V-5Fe (wt. %) alloy that was used in aircraft fasteners. Difficulties in processing and inconsistencies in heat treatment response of some early beta Ti alloys led to the development in the late 1960's and early 1970's of near-beta and metastable beta Ti alloys primarily for the aerospace industry [21,36,58]. The Ti-8V-8Mo-2Fe-3Al (wt. %) or Ti-8823 alloy, which has a MoE value of 16.2, was developed for high-strength forgings. The near-beta Ti-10V-2Fe-3Al (wt. %) alloy, which has a MoE value of 9.5, was developed for high-strength forgings in aircraft structures. The near-beta Ti-11.5Mo-6Zr-4.5Sn (wt. %) or Beta III alloy, which has a MoE value of 9.0 was developed for high-strength applications. Other metastable beta Ti alloys developed at this time include the Ti-3Al-8V-6Cr-4Zr-4Mo (wt. %) or Beta C alloy, which has a MoE value of 16.0, for use in aircraft springs and oilfields; the Ti-15V-3Al-3Sn-3Cr (wt. %) alloy, which has a MoE value of 10.9 for use in aircraft sheet and plate; and the Ti-15Mo-3Al-3Nb-0.2Si (wt. %) or Beta 21S alloy, which has a MoE value of 12.8, for use in oxidation-resistant metal matrix composites (MMCs). Some of these alloys found commercial application in low quantities. The Ti-15Mo-3Al-3Sn-3Cr (wt. %) alloy was used in the B-1B bomber's nacelles and empennage spars in the 1980's [62]. This alloy was selected since it was strip producible at low cost and has good formability compared to the Ti-6Al-4V (wt. %) alloy. In addition, it could be solution treated and aged to tensile strengths of 1034 MPa (150 ksi) or higher. The Ti-10V-2Fe-3Al (wt. %) alloy was used in the Boeing 777 landing gears [62]. It was used to provide weight savings compared to high-strength low-alloy steels such as 4340 or 300 M. The alloy was later used in Airbus aircraft. The most recently developed successful modern commercial alloy is the near-beta Ti-5Al-5Mo-5V-3Cr (wt. %) or Ti-5553 alloy, which has a MoE value of 8.2, for use in the aircraft structures and landing gears of the Boeing 787. Details on production status, physical properties, processing are found in product specification data from manufacturers and several articles in the existing literature [21,60,63,64]. Recently, several novel experimental alloys with high strengths and acceptable ductility have been reported in the literature. These include the near-beta Ti-7Mo-3Nb-3Cr-3Al (wt. %) alloy, which has a MoE value of 9.6 [65,66]; the metastable Ti-4.5Al-6.5Mo-2Cr-2.6Nb-2Zr-1Sn (wt. %) alloy known as TB17, which has a MoE value of 5.3 [67]; the near-beta Ti-4Al-7Mo-3Cr-3V (wt. %) alloy, which has a MoE value of 9.8 [68]; and the metastable Ti-3.5Al-5Mo-6V-3Cr-2Sn-0.5Fe (wt. %) alloy, which has a MoE value of 11.1 [69,70]. The mechanical properties of these newly developed alloys make them potential candidates for aircraft structures but only a few studies on the processing–structure–property relationships are reported in the existing literature.

3.2. Biomedical Implants

The development of metastable beta Ti alloys for biomedical applications represents the other significant effort in this class of alloys. The history of these alloys used in biomedical applications is more recent compared to use in aircraft structures and can be divided into development for orthopedic implants and orthodontics [11,13]. Alloys for orthodontics can be further categorized into those for devices (appliances) or wires and those for dental implants.

Early orthopedic implant alloys were primarily either cp α-Ti or Ti-6Al-4V (wt. %) extra-low interstitials (ELI) alloys [6,7,10,22]. But these alloys were initially developed for aircraft structures. Their good biocompatibility and corrosion resistance led to their use in orthopedic implants. However, concerns with the long-term cytotoxicity of V and Al ions released from implants led to modifications of the Ti-6Al-4V (wt. %) composition. Vanadium is known to have toxic effects in the V^{4+} and V^{5+} elemental state and as oxides such as V_2O_5 leading to adverse reproductive and developmental effects in mammals [71]. Although generally considered less toxic than V, the presence of Al in implants has been associated with the induction of neurotoxicity and age-related neurodegenerative diseases such as Alzheimer's disease [72,73]. Furthermore, research has suggested that Ti-6Al-4V (wt. %) implants may cause oxidative stress and prolonged inflammation [74] and osteolysis [75]. These concerns led to the development in the 1980's of dual-phase α + β Ti alloys without V including Ti-6Al-7Nb (wt. %) and Ti-5Al-2.5Fe (wt. %) alloys that had similar phase volume fraction ratios as Ti-6Al-4V (wt. %) [7,10,11,76]. However, α + β Ti alloys generally have lower notched fatigue resistance and poorer wear characteristics compared to metastable beta Ti alloys [75]. Another consideration is the modulus of elasticity mismatch between α + β Ti alloys, which is approximately between 110 GPa and 115 GPa, and cortical bone, which is approximately 30 GPa [11,30]. The stiffer implant carries the load rather than the bone, which atrophies and loses density (osteopenia) due to lack of functional stimulation in a process known as stress shielding [77]. This process may in turn lead to fractures or loosening of the implant. The desire to eliminate potentially toxic elements, reduce the modulus mismatch between the implant and cortical bone, and improve the wear characteristics of Ti implants led to the development of metastable beta Ti alloys for use in orthopedic implants [6,12,76]. Of the many beta phase stabilizing elements Nb, Ta, Zr, Mo, and Sn have been identified as having good biocompatibility with low toxicity and better corrosion properties compared to other elements [6,7,12,75,78]. Several metastable beta Ti alloys were simultaneously developed in the 1990's using these elements for use in implants. Kuroda et al., studied ternary Ti-29Nb-13Ta (wt. %) alloy, which has a MoE value of 11.0, and several quaternary variations by adding Zr, Mo, or Sn [12]. The Ti-29Nb-13Ta-4.6Zr (wt. %) alloy, which has a MoE value of 10.2, was developed further for commercial application by Niinomi et al. [22] Other metastable beta, near-beta, and beta-rich Ti alloys developed at this time for use in orthopedic implants include Ti-12Mo-6Zr-2Fe (wt. %) alloy, which has a MoE value of 16.8; Ti-13Nb-13Zr (wt. %) alloy, which has a MoE value of 1.4; and Ti-35Nb-5Ta-7Zr (wt. %) alloy, which has a MoE value of 9.7; and Ti-15Mo (wt. %), which has a MoE value of 15.0 [8,10,76,79–81]. In addition to the use of less toxic elements, these alloy have much lower modulus of elasticity that is closer to cortical bone reducing the effects of stress shielding, Figure 5. One important aspect of beta Ti alloys is the ability to tune the modulus of elasticity over a wide range by altering the composition and also the phase volume fraction through processing and heat treatment. More recently, several new experimental metastable beta Ti alloys have been developed including Ti-35Nb-7Zr-6Ta-(0-2)Fe-(0-1)Si (wt. %) [30], Ti-8Mo-(4-6)Nb-(2-5)Zr (wt. %) [31], Ti-33Nb-4Sn (wt. %) [82] in efforts to further lower the elastic modulus. In addition, binary Ti-Mn alloys are being investigated to lower costs associated with expensive Nb and Ta alloying elements [83]. These new experimental alloys require further study since little is known of their processing–structure–property relationships and the existing literature contains few studies compared to other beta Ti alloys.

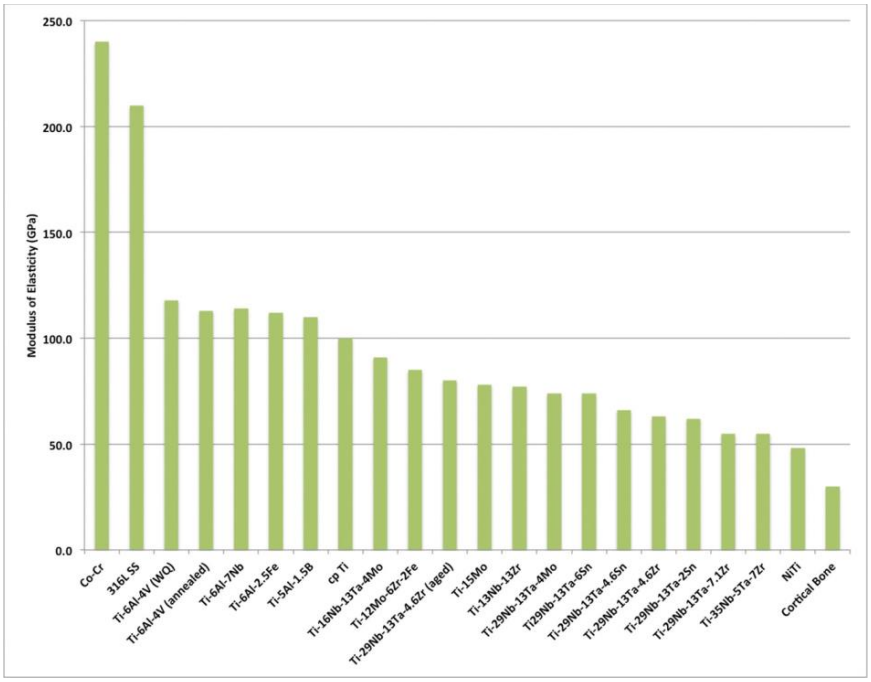

Figure 5. A plot showing the modulus of elasticity, *E*, (GPa) of commercially important and experimental Ti alloys used in orthopedic implants. The quantity *E* for Co-Cr, 316L stainless steel, and cortical bone are also shown.

Orthodontic alloys for devices and wires have the same requirement as orthopedic alloys for low toxicity, biocompatibility, good corrosion resistance, good formability, and good weldability. However, orthodontic alloys also require high spring-back and low stiffness to apply lighter and more constant forces to move teeth. Early orthodontic alloys were traditionally stainless steels and Ni-Cr-Co alloys. Goldberg and Burnstone published the first study evaluating metastable beta Ti alloys for orthodontic appliances and wires in 1979 [84,85]. These authors demonstrated that the near-beta Ti-11.5Mo-6Zr-4.5Sn (wt. %) alloy, which has a MoE value of 9.0, had excellent potential as a replacement material for 18-8 austenitic stainless steel if properly thermo-mechanically processed. This alloy is known as "TMA" and was produced under exclusive patent by Ormco until recently. In wire form, this Ti alloy has a lower modulus of elasticity and a higher yield strength-to-modulus ratio, which results in clinically desirable lower forces and greater elastic recovery (spring-back). Goldberg and Shastry studied the age hardening characteristics of this alloy and also the metastable Ti-13V-11Cr-3Al (wt. %) alloy [86] demonstrating the ability to tune the modulus of elasticity through heat treatment. Wilson and Goldberg investigated alternative beta titanium alloys for orthodontic wires including the metastable Ti-3Al-8V-6Cr-4Mo-4Zr (wt. %) alloy, the metastable Ti-15V-3Cr-3Al-3Sn (wt. %) alloy, and the near-beta Ti-10V-2Fe-3Al (wt. %) alloy [87]. These authors illustrated that the Ti-15V-3Cr-3Al-3Sn (wt. %) alloy may be suitable for clinical use in orthodontic wires. One disadvantage of the TMA alloys is its propensity to fracture and some studies have examined the biocompatibility, corrosion resistance, and fracture characteristics of these alloys [88]. The expiration of the patent for the TMA alloy has led to the introduction of many modified TMA alloys that are being evaluated for use in orthodontic devices and wires [89–92]. More recently, a study by Hida et al., has reported on the development of the experimental near-beta Ti-6Mo-4Sn (wt. %) alloy, which has a MoE value of 4.7 for use in orthodontic wires for transpalatal arches [32]. These authors primarily examined the effect of heat treatment on tensile strength and thus this alloy has only been studied to limited extent. Further research is required on its fatigue properties, cytotoxicity, and biocompatibility. Despite the renewed recent interest in beta Ti alloys, other metal material systems

such as Ni-Cr-Co alloys, NiTi shape memory alloys, and Cu-Ni-Ti alloys are also used to fabricate orthodontic devices and wires providing significant competition.

Modern dental implant alloys are primarily either cp α-Ti or Ti-6Al-4V (wt. %) ELI alloys due to their good biocompatibility, corrosion resistance, and osseointegration [93]. A dental implant is in general an artificial tooth that is integrated with a titanium screw of tapered geometry for anchoring into the jaw. The surface of the screw may be modified or coated to provide improved biocompatibility or osseointegration. The use of titanium as dental implants started in the early-to-mid 1960's when Brånemark and his colleagues performed in vivo studies of titanium implants in dog and rabbit animal models [94]. These experiments led to the concept of bone-anchored bridge ca. 1965 [95,96]. Brånemark also introduced the concept of osseointegration after observing that titanium implants firmly embed into the bone of animal models [94]. Furthermore, no inflammation was observed around these titanium implants. However, there have been numerous attempts to further improve the properties cp α-Ti or Ti-6Al-4V (wt. %) ELI, especially those related to elastic modulus, corrosion resistance, and biocompatibility. Furthermore, the potentially detrimental long-term effects of V and Al have been noted above [71–73], and researchers are attempting to replace these elements in dental implant alloys. One experimental candidate is the near-beta Ti-20Nb-10Zr-5Ta (wt. %) alloy also known as "TNZT", which has MoE value of 5.0. Moreover, metals like Nb, Ta, and Zr are thought to have good biocompatibility and osteoconductivity with no known adverse effect on the human body [6,7,12,75,78]. The TNZT alloy has a modulus of elasticity of 59 GPa more closely matching that of cortical bone and reportedly has low cell toxicity [97]. Although a few papers are found in the existing literature, these have mostly studied biocompatibility. The processing–structure–property relationships of the TNZT alloy are not adequately addressed in the existing literature and require further research to evaluate its biomechanical properties for implants. In addition, Niinomi reports that beta Ti alloys have been investigated in Japan for use in dental castings [83].

4. Titanium Alloy Production, Thermo-Mechanical Processing, and Heat Treatment

In spite of mechanical property, corrosion resistance, and biocompatibility benefits offered by beta titanium alloys, their direct usage is predominantly hampered by their high extraction and processing costs. In general titanium alloys have been traditionally produced through either the Hunter process or Kroll process [98]. The Hunter process is defined by following reaction:

$$4Na\ (liquid) + TiCl_4\ (gas) \rightarrow 4NaCl\ (Liquid) + Ti\ (solid\ at\ 700\ ^\circ C–800\ ^\circ C).$$

The use of sodium (Na) and high-energy consumption during electrolysis of NaCl significantly increases the cost of this processing route. Hence this process was replaced by the Kroll process, which uses magnesium (Mg) instead of Na for reduction [99]. The Kroll process is defined by the following reaction:

$$2Mg\ (liquid) + TiCl_4\ (gas) \rightarrow 2MgCl_2\ (liquid) + Ti\ (Solid\ at\ 800\ ^\circ C–850\ ^\circ C),$$

and used by many commercial producers of titanium alloys. One of the main challenges for the Kroll process is removal of $MgCl_2$ entrapped within the Ti sponge. That Ti sponge that is formed is extremely strong and not amenable to crushing. This requires an extra step where the Ti sponge is cut, bored, sheared, and crushed to release the entrapped $MgCl_2$. This additional step of purifying the Ti sponge is a time consuming step that adds significant cost to the process producing titanium alloy.

The high cost of conventional Ti alloy production aided motivation of novel research on near net shape processing of titanium alloys through solid-state powder processing [100]. Powder production processes have recently been developed that provide cost savings in comparison to the Kroll process. Within the various powder processing pathways for beta Ti alloys, the TiH_2 powder process has demonstrated potential for producing large beta Ti alloy parts with good compositional and microstructural qualities [101,102]. The TiH_2 powder is produced by cooling through a metallothermic

reduction of $TiCl_4$ in a hydrogen atmosphere. The TiH_2 powder is mixed with different alloy powders and cold compacted and sintered in vacuum at a temperature above 400 °C, leading to hydrogen evolution, reduction of any oxides, and formation of alloy rods. The brittle TiH_2 powder is easily ground, unlike titanium sponge produced through traditional methods lowering costs and reducing energy consumption. Joshi et al., have produced billets of metastable beta Ti-1Al-8V-5Fe (wt. %), which has a MoE of 18.9, and then performed thermo-mechanical processing. After aging, the alloy has hierarchical nanostructure with high tensile strength greater than ~1500 MPa, Figure 6 [103]. The lower cost TiH_2-based powder processing method may lead to increased adoption of beta Ti alloys for engineering applications.

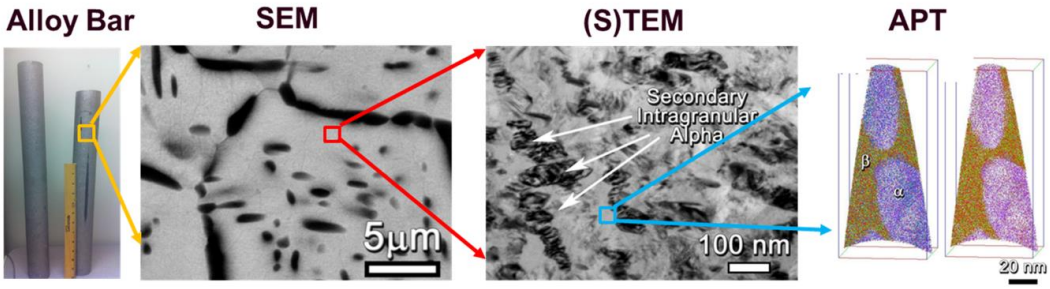

Figure 6. The microstructure and nanostructure of a metastable Ti-1Al-8V-5Fe (wt. %) alloy with a hierarchical nanostructure achieved by sub-transus solution heat treatment and isothermal aging. The alloy powder feedstock was processed by the TiH_2 based powder process.

Metastable beta (and near-beta) Ti alloys are typically thermo-mechanically processed and heat-treated to obtain the desired microstructure, phase volume fraction, and mechanical properties for an engineering application [51,58,104]. In context of metastable beta Ti alloys, thermo-mechanical processing is the use of hot deformation, water quenching, and air cooling to alter the shape and microstructure, whereas heat-treatment is defined as solution treatment followed by aging to affect strength; or annealing to relieve residual stresses or improve fabricability. Thermo-mechanical processing can be further sub-divided into primary or secondary processing as discussed below. Solution treatment and aging is performed after secondary processing. Metastable beta Ti alloys have excellent workability due to their lower beta transus temperature compared to dual-phase $\alpha + \beta$ Ti alloys such as Ti-6Al-4V (wt. %) and thus they are more easily forged, rolled, and extruded. Furthermore, they are deeply hardenable, which means that their strength can be increased significantly by solution treatment and aging. This combination has led to their processing by hot near net-shape forging methods for use in aircraft structures and other high performance engineering applications. Additionally, these alloys may also be cold worked, which is performed at a temperature significantly below the quantity T_β [1].

4.1. Thermo-Mechanical Processing

Metastable beta Ti alloys are thermo-mechanically processed to produce useable shapes for engineering applications, optimize mechanical properties by controlling the microstructure, and to delay or suppress the formation of the embrittling isothermal ω-phase during aging [34,58,104]. Sauer and Luetjering also state that another significant purpose is to prevent or limit the formation of continuous α-phase along the β-phase grain boundaries [104]. This morphology has a detrimental effect on some mechanical properties, especially in the case of large equiaxed β-phase grains. Thermo-mechanical processing is broadly categorized into two steps by Weiss and Semiatin [58]. The first or primary processing step is typically performed at temperatures above the quantity T_β in the single β-phase field to breakdown the ingot structure and produce plate, bar, rod, or other similar mill products. The second or secondary processing step is performed at temperatures slightly above the quantity T_β in the single β-phase field (super-transus) or slightly below the quantity T_β in the $\alpha + \beta$

phase field (sub-transus) depending on the desired microstructure and properties. Weiss and Semiatin have listed several metastable beta Ti alloys with their hot deformation temperature ranges for ingot breakdown and secondary processing steps [58]. The hot deformation temperatures depend on the alloying content and the beta phase stability. In general, the greater the MoE value and bcc β–phase stability, the lower the quantity T_β which in turn reduces the hot deformation temperatures used in the thermo-mechanical processing steps. A list of beta transus temperatures of several commercially important metastable and near-beta Ti alloys is provided in Table 2. A list of beta transus temperature ranges for other beta Ti alloys primarily used in aircraft structures and engines are found in the text by Donachie [52], the article by Weiss and Semiatin [58], the article by Cotton et al. [21], and the article by Nyakana et al. [60]. In the discussion that follows we focus on secondary thermo-mechanical processing of metastable beta Ti alloys for aerospace applications, which requires high specific strength and good ductility and thus careful control of the processing temperatures and parameters. Thermo-mechanical processing of biomedical implants is briefly addressed at the end of the section.

The secondary processing step involves a combination of heating, cooling, and deformation such as in isothermal forging to produce a shape that is near the final one used in an engineering application. The result of hot deformation in the single β-phase field is to form large β-phase grains. The α-phase along the grain boundaries may be continuous or form in short segments depending on the cooling rate [104]. On the other hand significant hot deformation in the $\alpha + \beta$ phase field forms larger equiaxed (globular) primary α-phase particles that pin the β-phase grain boundaries limiting their growth during recrystallization. The β-phase grains are thus small and in turn the lengths of continuous α-phase along the grain boundaries are short [104]. The differences are illustrated for the commercially important near-beta Ti-10V-2Fe-3Al (wt. %) alloy in Figure 7a,b [105]. In Figure 7a, the alloy was forged in the single β-phase field resulting in large β-phase grains of approximately 300 µm diameter. The beta grains contain a high volume fraction of Widmanstätten α-phase plates, and almost continuous grain boundary α-phase indicating that the cooling rate after forging was relatively slow. In Figure 7b, the alloy was forged in the $\alpha + \beta$ phase field about 100 °C below the beta transus temperature forming a high volume fraction of globular primary α-phase particles. The bcc β-phase grains are much smaller and hence the grain boundary α-phase segments are shorter.

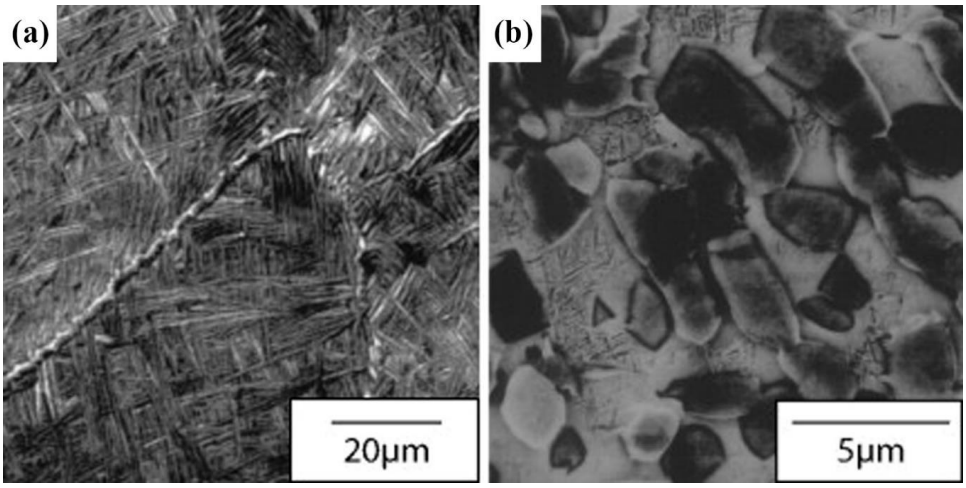

Figure 7. The differences in microstructure between hot forging in the single β-phase field in (**a**) and the $\alpha + \beta$ phase field in (**b**) are illustrated. The microstructure in (**a**) depicts large bcc β-phase grains with almost continuous grain boundary α-phase. The beta grains also contain a high volume fraction of Widmanstätten α-phase plates. The microstructure in (**b**) depicts smaller bcc β-phase grains with some martensite phases and large globular primary α-phase particles [105]. (Reprinted by permission from Materials Science and Engineering A, vol. 501, no. 1–2, M. Jackson, N. G. Jones, D. Dye, and R. J. Dashwood, Effect of initial microstructure on plastic flow behavior during isothermal forging of Ti–10V–2Fe–3Al, 248–254, 2009, with permission from Elsevier).

Studies have been performed to evaluate the plastic flow behavior as a function of processing parameters at both super-transus and sub-transus temperatures for near-beta and metastable beta Ti alloys [65–67,105–112]. The microstructural evolution, recrystallization texture, and mechanical properties of these alloys are very sensitive to the secondary processing parameters. The controllable process variables are temperature, heating rate, cooling rate, strain rate, and strain. In general, during hot deformation in the β-phase field the stress vs. strain curves exhibit a very sharp initial peak at very low strains followed by a yield drop, in a phenomenon known as discontinuous yielding. This is followed by an almost steady-state stress deformation [58]. The discontinuous yielding phenomenon has been related to the rapid generation of mobile dislocations from grain boundaries leading to deformation from the grain boundary towards the interior of the grain. The extent of this effect depends on the strain rate, grain size, and alloy composition. High strain rates produce a larger drop in yield. Fine-grained alloys have a greater yield drop magnitude due to a larger number of grain boundaries. Additionally, the magnitude of the yield drop is influenced by the type and concentration of beta phase stabilizing elements and thus the MoE values. There is a general trend of increasing magnitude of yield drop with increasing MoE value [109]. The magnitude of the peak stress decreases with increasing temperature, decreasing strain rate, and increasing grain size. Higher steady-state flow stresses are observed at higher strain rates and lower deformation temperatures as shown. On the other hand, during hot deformation in the $\alpha + \beta$ phase field, the stress vs. strain curves exhibit rapid work hardening to a peak followed by flow softening at an exponential rate and subsequently attains steady-state flow at high strains [58]. The general differences in stress vs. strain curves between the two deformation regimes are illustrated for the near-beta Ti-5Al-2Sn-2Cr-4Mo-4Zr-1Fe (wt. %) alloy in Figure 8a,b [58]. The quantity T_β is approximately 890 °C (1634 °F) for this alloy. In addition to the effect of the aforesaid parameters the plastic flow behavior during secondary processing is influenced by the initial microstructure of each alloy. Jackson et al., have studied the effect of initial microstructure on the plastic flow stresses in the Ti-10V-2Fe-3Al (wt. %) alloy during sub-transus isothermal forging [105]. Their study illustrated that a microstructure with high aspect ratio Widmanstätten α-phase platelets produces greater sub-transus flow stresses compared to a microstructure with large globular primary α-phase using the same hot deformation parameters. The microstructure also influences the magnitude of work hardening and flow softening depending on the strain rates. This difference is primarily due to dislocation pile-up at the heterophase α-phase/β-phase interfaces of the Widmanstätten platelets and subsequent break-up of the platelets that is related to the extent of flow softening. Jones et al., performed a similar study of the effect of microstructure on the plastic flow stresses in the metstable Ti-5Al-5Mo-5V-3Cr (wt. %) during sub-transus isothermal forging [107]. They reported results qualitatively similar to Jackson et al., Zhao et al., also investigated the plastic flow behavior in Ti-10V-2Fe-3Al (wt. %) during super-transus isothermal forging [109]. Their results demonstrated that discontinuous yielding occurs at all the studied temperatures and strain rates. But the effect is more pronounced at high strain rates of 0.1 s^{-1} than at lower strain rates of 0.01 s^{-1} and 0.001 s^{-1}. The plastic flow is dominated by dynamic recovery at super-transus temperatures for this alloy. Due to the commercial importance of these two alloys other recent studies on the relationship between the plastic flow behavior and processing parameters have been performed on Ti-10V-2Fe-3Al (wt. %) by Lei et al. [110], and on Ti-5Al-5Mo-5V-3Cr (wt. %) by Hua et al. [108] Lei et al., studied hot deformation at higher super-transus temperatures between 800 °C and 1150 °C and a wider range of strain rates between 0.001 s^{-1} and 10 s^{-1} with controlled cooling that formed a martensitic microstructure. These authors illustrated that the volume fraction of martensite was a function of both strain rate and deformation temperature. Through proper selection of strain rate and deformation temperature they demonstrated that it was possible to avoid the formation of the martensitic phases in this alloy. Hua et al., investigated dynamic recovery at temperatures between 750 °C and 900 °C and at strain rates between 0.001 s^{-1} and 0.1 s^{-1}. Their results indicate that dynamic recrystallization is greater at higher temperatures and lower strain rates and that the quantity of low-angle grain boundaries increases significantly during hot deformation. The study by Hua et al., also illustrated that the volume

fraction of secondary α-phase precipitates increases during aging after hot deformation, which is most likely caused by increased heterogeneous nucleation sites. Warchomicka et al. [111] studied dynamic recrystallization in the related Ti-5Al-5Mo-5V-3Cr-1Zr (wt. %) alloy at strain rates between 0.001 s^{-1} and 0.1 s^{-1} and temperatures near the quantity T_β = 803 °C. This alloy is reportedly used in the Airbus 380 aircraft [21]. They observed similar results to the study by Hua et al. Due to the commercial importance of Ti-10V-2Fe-3Al (wt. %) and Ti-5Al-5Mo-5V-3Cr (wt. %) alloys several other recent studies have been reported in the literature [112–114] and research on these alloys remains an important topic.

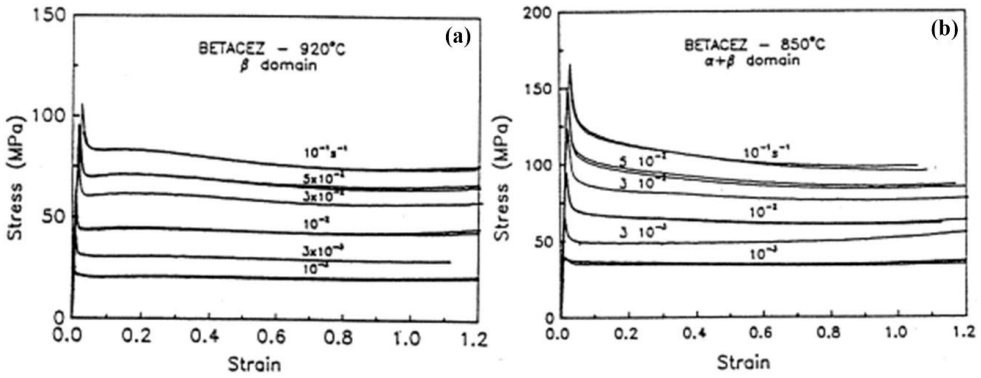

Figure 8. An illustration of the differences in hot deformation plastic flow curves for the Ti-5Al-2Sn-2Cr-4Mo-4Zr-1Fe (wt. %) alloy referred to as Beta CEZ at 920 °C (super-transus) in (**a**) and at 850 °C (sub-transus) in (**b**). The quantity T_β is approximately 890 °C for this alloy [58]. (Reprinted by permission from Materials Science and Engineering A, vol. 243, no. 1–2, I. Weiss and S. L. Semiatin, Thermomechanical processing of beta titanium Alloys—an overview, 46–65, 1998, with permission from Elsevier).

More recently, a few studies have reported on the high-temperature deformation behavior of newly developed or experimental alloys for aerospace applications. This includes the near-beta Ti-7Mo-3Nb-3Cr-3Al (wt. %), which has an ultrahigh tensile strength of >1350 MPa and moderate ductility of > ~8% [65,66]; and the metastable Ti-4.5Al-6.5Mo-2Cr-2.6Nb-2Zr-1Sn (wt. %), which has a higher tensile strength of >1400 MPa and moderate ductility of > ~7% [67]. However, only a few studies on thermo-mechanical processing of theses alloys are found in the extant literature and thus further studies must be performed in order to gain greater understanding of their thermo-mechanical processing response before commercial application.

The objective of these aforementioned studies is to determine each alloy's optimal secondary processing temperatures and parameters for a set of desired mechanical properties. Despite the general trends for these alloys, differences in composition, MoE values, and microstructure lead to distinctive processing temperatures and parameters depending on the application. For instance, the commercially important near-beta Ti-10V-2Fe-3Al (wt. %) alloy is primary processed in the single β-phase field followed by lower temperature finishing in the α + β phase field at a temperature approximately between 10 °C and 25 °C below the beta transus temperature [21,62,105,106]. The amount of deformation or work in the α + β phase field is a function of the desired properties and trade off between fracture toughness and ductility. If good fracture toughness is required, then minimal α + β forging will be performed, forming a microstructure with large β-phase grains and primary Widmanstätten α-phase platelets. The ductility is, however, low with this microstructure and is further limited by the presence of greater amounts of continuous grain boundary α-phase. However, if good ductility is desired, then greater α + β deformation will be performed recrystallizing some of the Widmanstätten α-phase platelets and breaking down the grain boundary α-phase forming small volume fractions of primary equiaxed (or globular) α-phase precipitates. The relationship between the ductility in % reduction of area (%RA) and fracture toughness, K_{Ic}, and the amount of work in α + β phase field

for this alloy is illustrated in Figure 9a,b [106]. On the other hand, the metastable Ti-5Al-5Mo-5V-3Cr (wt. %) alloy is an example of an alloy that may be primary processed in the single β-phase field or the $\alpha + \beta$ phase field depending on the desired fracture toughness and ductility before finish forging in the $\alpha + \beta$ phase field [107]. Greater ductility and fracture toughness are achieved when primary forging is performed above the quantity T_β. However, the ability to perform primary processing below the beta transus temperature is simpler and less costly.

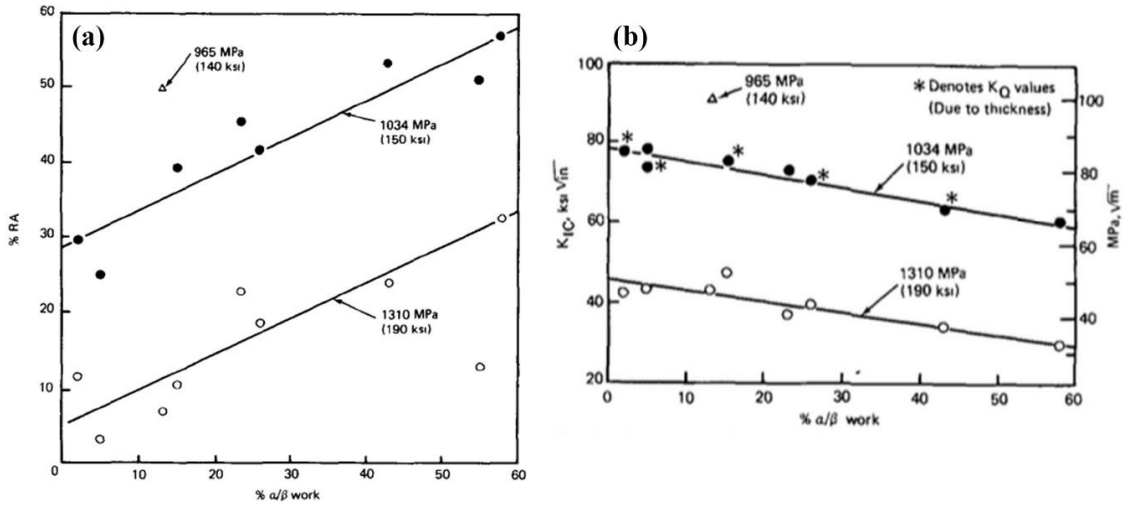

Figure 9. For the near-beta Ti-10V-2Fe-3Al (wt. %) alloy, the relationship between the amount of work in the $\alpha + \beta$ phase field and ductility is illustrated in (**a**) and fracture toughness is shown in (**b**) [106]. (Reprinted by permission from Metallurgical Transaction A, vol. 18, no. 12, R. R. Boyer and G. W. Kuhlman, Processing properties relationships of Ti-10V-2Fe-3Al, 2095–2103, 1987, with permission from Springer Nature).

Alloys used for biomedical applications may also be thermo-mechanically processed but in general, the strength requirements are much lower and thus these have received much less attention in the literature. The focus of alloys used in orthopedic and orthodontic applications is instead the modulus of elasticity, cytotoxicity, corrosion resistance, and biocompatibility. Several studies on the relationship between thermo-mechanical process and microstructural evolution in biomedical alloys have, however, been reported in the literature. Geetha et al., were the first to provide a detailed investigation of the near-beta Ti-13Nb-13Zr (wt. %) alloy [11]. These authors studied sub-transus hot deformation followed by solution treatment in either the single β-phase field or the $\alpha + \beta$ phase field and then isothermal aging. They later reported on the near-beta Ti-20Nb-13Zr (wt. %) and Ti-20Nb-20Zr (wt. %) alloys [115]. More recently, other researchers have studied hot deformation and microstructural evolution of the Ti-13Nb-13Zr (wt. %) alloy in an effort to tune the microstructure and mechanical properties for orthopedic implants [116–119]. Of the several metastable or near-beta biomedical alloys, studies on thermo-mechanical processing of the Ti-13Nb-13Zr (wt. %) alloy are found most frequently in the literature possibly due to its low beta transus temperature of 735 °C (1355 °F) [120].

4.2. Heat Treatment

In general, heat treatment of metastable beta Ti alloys is performed to relieve residual stresses, improve the ability to fabricate a near net shape part, or strengthen the part through precipitation of secondary hcp α-phase. Heat treatment may also be used to improve ductility, fracture or impact toughness, and corrosion resistance.

4.2.1. Stress Relief Annealing

Undesirable residual stresses may occur during non-uniform hot deformation, cold working, asymmetric machining operations, and welding. Heat treatment to relieve residual stress may be performed as an intermediate step during thermo-mechanical processing after its completion. Stress relief annealing is often performed at sub-transus temperatures in the $\alpha + \beta$ phase field followed by air-cooling. Water or oil quenching may lead to additional undesirable residual stresses. For example, the metastable Ti-5Al-5Mo-5V-3Cr (wt. %) alloy is stress relief annealed at between 650 °C (1202 °F) and 750 °C (1382 °F) for a minimum of 4 h followed by air-cooling [21]. Donachie lists a few metastable and near-beta Ti alloys and their stress-relief temperature and time ranges [52]. Higher temperatures can be used with shorter times and lower temperatures with longer times. By selecting appropriate temperatures and times, stress relief annealing can be performed without changing the microstructure, causing significant recrystallization, or adversely altering strength or ductility. Stress relief annealing of many metastable or near-beta Ti alloys is performed after thermo-mechanical processing but simultaneously with solution treatment and aging. For example, the near-beta Ti-10V-2Fe-3Al (wt. %) alloy is water-quenched after solution treatment 750 °C (1382 °F) in order to achieve good mechanical properties during aging [21]. But water quenching produces significant residual stresses that affect dimensional stability during machining. For this alloy, isothermal aging is usually performed at between 495 °C and 525 °C for 8 h to precipitate a high number density of the secondary hcp α-phase precipitates followed by an air cool, and this heat treatment also serves to relieve residual stresses in the alloy.

4.2.2. Annealing to Improve Fabricability

Heat treatment to improve fabricability may be performed as intermediate steps during thermo-mechanical processing, especially for parts requiring significant reductions in cross-sectional area such as sheet, wire, or fasteners. Annealing to improve fabricability is often performed at slightly below the quantity T_β followed by a water quench or air cool. In general, metastable beta Ti alloys possess high ductility and low plastic flow strength at this temperature in the $\alpha + \beta$ phase field making it suitable for hot deformation. The annealing duration is predominantly a function of the part thickness. For instance, the near-beta Ti-5Al-5Mo-5V-3Cr (wt. %) alloy is solution annealed at between 20 °C and 60 °C below the quantity T_β for a minimum of 1 h followed by air cooling [21]. In some cases, annealing can be performed in the single β-phase field at temperatures between 20 °C and 60 °C above the quantity T_β. Annealing in the single β-phase field for too long can, however, result in excessive grain growth of the bcc β-phase, leading to large grains with continuous grain boundary α-phase and deleterious effect on mechanical properties [104]. Donachie lists a few metastable and near-beta Ti alloys and their annealing temperature and time ranges [52].

Annealing may also improve the ability to cold work some commercial beta Ti alloys. Karasevskaya et al., demonstrated that metastable Ti-15V-3Cr-3Al-3Sn (wt. %) and Ti-7Mo-5Fe-2Al (wt. %) alloys have improved colds workability after super-transus solution treatment for 0.5 h [121]. This produced a completely recrystallized microstructure with bcc β-phase grain diameters of 150–200 µm. The improved ability to perform cold work was related to the formation of well-defined sub-grain and cell structure. Straining proceeds readily by means of deformation and rotation within and adjacent to sub-grains and cells. Hence, deformation is easily accommodated, intragranular stresses are low, and hence ductility is high. On the other hand, the near-beta Ti-5Mo-5V-5Al-1Fe-1Cr (wt. %) known as "VT-22" and the near-beta Ti-7V-4Mo-3Al (wt. %) alloy known as "TC6" do not have improved cold workability [121]. This was related to poorly defined sub-grain and cell structure. Deformation during cold working is limited by large intragranular stresses resulting from multi-component textures and stress-induced transformations. Studies on stress-induced transformations at ambient (room) temperature is a subject of many current research efforts and is reviewed below.

4.2.3. Solution Treatment and Aging

The optimal microstructure and mechanical properties for an engineering application can be obtained for a metastable or near-beta Ti alloy by solution treatment and aging after thermo-mechanical processing. Strengthening or hardening by solution treatment and aging in beta Ti alloys obeys conventional solutionizing, supersaturation, and precipitation theory for most alloys [122]. The ability to strengthen a metastable or near-beta Ti alloys during solution treatment and aging is related to the instability of the bcc β-phase at temperatures below the quantity T_β. This is also related to the concept of hardenability of a beta Ti alloy, which is defined by Cotton et al., as the ability to produce an age-hardening response from the supersaturated β-phase [21]. Analogous to ferrous alloys, the thicker the section that can retain the metastable β-phase, the higher the hardenability of the beta Ti alloy. The hardenability can be measured by a modified Jominy End Quench test but only a few studies are present in the extant literature [123]. In order for a beta Ti alloy to be hardenable, the hcp α'-martensite phase and the orthorhombic α''-martensite phase must be suppressed during solution treatment and quenching permitting the alloy to exist predominantly of the bcc β-phase in a supersaturated state. Furthermore, secondary α-phase precipitates should not form during quenching. The formation of martensitic phases is avoided by alloying with sufficient beta phase stabilizing elements to lower the Ms temperature shown schematically in Figure 2 and discussed above. In general avoiding precipitation of the secondary α-phase is dependent on slowing the precipitation kinetics. One route is to include slow diffusing beta phase stabilizing elements such as V, Mo, and Nb. However, as the MoE value increases and the quantity T_β is lowered, the ability to strengthen by aging is concomitantly reduced. For instance, the stable Ti-35V-15Cr (wt. %) alloy does not need to be quenched to retain the β-phase and furthermore it does not form significant quantities of secondary α-phase during aging due to its high MoE value of 47.5 [21].

Solution Treatment

Solution treatment may be performed at super-transus temperatures or sub-transus temperatures. In either case, the alloy is heated to a sufficiently high temperature then soaked followed by rapid quenching or cooling to ambient or room temperature. Depending on the desired properties and application some alloys can be used in the solution-treated state such as the metastable Ti-13V-l1Cr-3Al (wt. %) alloy, which was used in the SR-71 "Blackbird" aircraft. In a second example, the Ti-15Mo-3Al-3Nb-0.2Si (wt. %) alloy is usually supplied in the single β-phase solution treated condition permitting it to be easily cold worked [21]. After cold working this alloy is aged at the appropriate temperature and time for the desired mechanical properties. Most alloys are, however, aged after solution treatment and quenching to achieve the desired mechanical properties. Metastable beta Ti alloys that are more heavily stabilized and have high MoE values are usually solutionized at temperatures slightly above the quantity T_β, whereas metastable beta Ti alloys with lower MoE values and near-beta alloys are usually solutionized at temperature slightly below the quantity T_β. These two processes are categorized as beta solution treatment and alpha-beta solution treatment [34,52]. The difference between the two are depicted schematically for the illustrative case of solution treatment in the β-phase field followed by isothermal aging and for solution treatment in the $\alpha + \beta$ phase field followed by isothermal aging in Figure 10a,b. Beta solution treatment homogenizes the alloy forming a bcc β-phase microstructure. In this state, an alloy has low strength but high ductility. Solution treatment in the single β-phase field for too long can, however, result in excessive grain growth and coarsening of the bcc β-phase that negatively affects mechanical properties [104,124]. Alpha-beta solution treatment leads to enrichment of the bcc β-phase according to the lever rule for equilibrium phase diagrams. Small volume fractions of the intragranular primary hcp α-phase forms and also along the bcc β-phase grain boundaries. The primary α-phase pins the β-phase grain boundaries limiting their growth during solution treatment. In this state, an alloy usually has comparatively higher strength but lower ductility. In general, the size, morphology, and volume fraction of the primary

α-phase influence the mechanical properties, providing an important route to optimize the mechanical behavior of beta Ti alloys [124].

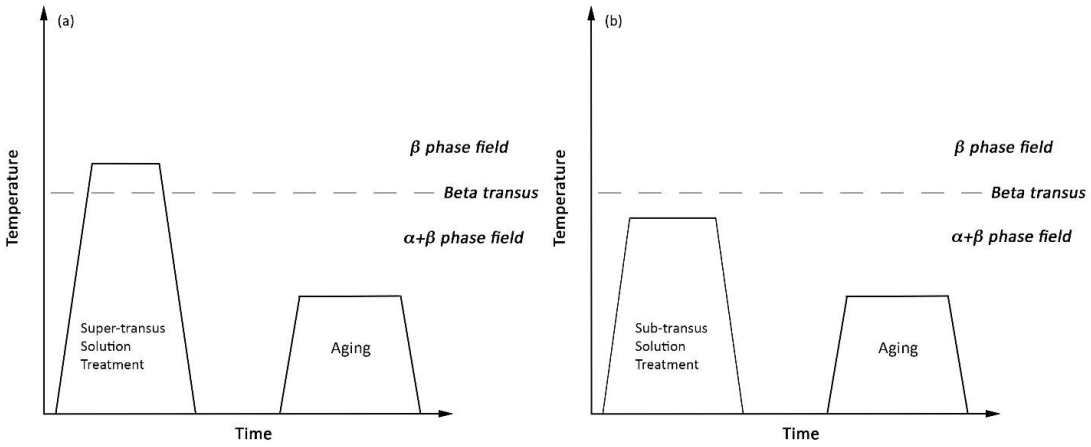

Figure 10. A schematic illustrating the qualitative difference between (**a**) super-transus solution treatment in the β-phase field and, (**b**) sub-transus solution treatment in the α + β dual-phase field followed by isothermal aging.

The metastable Beta C alloys, which has an MoE value of 16.0, is an example of an alloy that is solution treated at super-transus temperatures. This alloy is typically solution treated at between 790 °C (1454 °F) and 925 °C (1697 °F) for 0.5 h to 1 h followed by either air cooling, forced air cooling, or water quenching depending on section size [21]. The alloy can be used in only the solution treated condition or it may be subsequently aged depending on the desired strength and application. On the other hand, the near-beta Ti-5Al-5Mo-5V-3Cr (wt. %) alloy has several solution treatment options due to its larger processing window. This alloy may be solution treated at super-transus or sub-transus temperatures depending on the desired properties. Sub-transus solution treatment in the α + β phase field is usually performed at temperatures between 20 °C and 60 °C below the quantity T_β, which varies between 820 °C (1508 °F) and 880 °C (1616 °F) for a minimum of 1 h followed by air cooling [21]. Super-transus solution treatment is commonly performed at temperatures between 20 °C and 60 °C above the quantity T_β in the single β-phase field for a minimum of 1 h followed by air cooling. Cotton et al. also indicate that a double or modified solution treatment can be performed on this alloy where the aforesaid first step is followed by a second step solution treatment between 720 °C (1328 °F) and 790 °C (1454 °F) for 1 h to 3 h followed by air cooling. These conditions give the alloy greater ductility.

Several studies comparing the effects of super-transus and sub-transus solution treatment on the microstructure and mechanical properties of metastable and near-beta Ti alloys have been recently published in the literature. Srinivasu et al., investigated the effect of solution treatment temperatures on mechanical properties after super-transus and sub-transus thermo-mechanical processing in the near-beta Ti-10V-2Fe-3Al (wt. %) alloy [125]. These authors found that super-transus solution treatment regardless of thermo-mechanical processing temperatures led to lower ductility of <1% elongation compared to when solution treated at sub-transus temperatures. Furthermore, the authors determined that super-transus hot deformation followed by sub-transus solution treatment led to higher fracture toughness. The aforesaid differences were attributed to the two primary α-phase morphologies observed in the microstructure, which are the equiaxed morphology or a more acicular morphology. A study by Li et al., on the new metastable Ti-6Cr-5Mo-5V-4Al (wt. %) alloy, which has a MoE of 14.0, evaluated the effect of solution temperature on the microstructure and mechanical properties [126]. These authors reported that the alloy has a more attractive combination of strength and ductility when using alpha-beta solution treatment compared to beta solution treatment followed by isothermal aging. The alpha-beta solution treated alloy had bcc β-phase grains <10 µm in size with micron-scale primary α-phase and nano-scale secondary α-phase precipitates. The small β-phase grains combined

with the primary α-phase gave good ductility of 6–13.5% elongation and 22–52% reduction of area while the secondary primary α-phase provided high tensile strengths of 1400–1600 MPa. On the other hand, the beta solution treated alloys had bcc β-phase grains of between 40 µm and 100 µm in size and 1–5 µm secondary α-phase precipitates. The combination led to lower tensile strengths of 1200–1400 MPa and lower ductility of 7–10% elongation and 22–28% reduction of area. Another recent study by Du et al., on Ti-3.5Al-5Mo-6V-3Cr-2Sn-0.5Fe (wt. %) alloy examined the effect of solution heat treatment on the microstructure and tensile properties [69]. The observed similar results to Srinivasu et al., in that sub-transus solution treatment led to better ductility and finer grain size compared to super-transus solution treatment irrespective of hot rolling (deformation) temperature. Similar results were observed by Shekhar et al., in the near-beta Ti-5Al-5V-5Mo-3Cr (wt. %) alloy [127]. A study on the metastable Ti-1Al-8V-5Fe (wt. %) alloy, which has a MoE value of 18.9, by Devaraj et al., evaluated varying sub-transus solution treatment temperatures on tensile and fatigue properties [103]. These authors reported that solution treatment at a temperature closest to the quantity T_β gave the highest yield strength and tensile strength values, which was attributed to greater volume fraction of nanoscale secondary α-phase precipitates uniformly distributed in the bcc β-phase matrix. The authors also suggested that combination of primary hcp α-phase with a micron scale combined with the nanoscale secondary α-phase precipitates promoted higher strength. The effect of solution treatment remains one area of active research due to its influence on microstructure and mechanical properties and the sensitivity of beta Ti alloys to processing variations.

Aging

Aging after solution treatment leads to an increase in strength and hardness but a concomitant decrease in ductility. This occurs due to phase decomposition of the metastable bcc β-phase forming equilibrium secondary hcp α-phase precipitates. Super-transus or sub-transus solution treatment is followed by an aging heat treatment, Figure 10a,b. In general there are four aging methods, which are isothermal aging at high temperatures, isothermal aging at low temperatures, duplex (two-step) aging, or direct aging. The combination of sub-transus solution treatment followed by aging will result in primary α-phase and secondary α-phase precipitates with bimodal morphologies that often results in improved mechanical properties as discussed below. The difference between high temperature and low temperature aging in a pseudo-binary isomorphous phase diagram is shown in Figure 11. Modifications of the aforementioned four methods have also been presented in the literature [128].

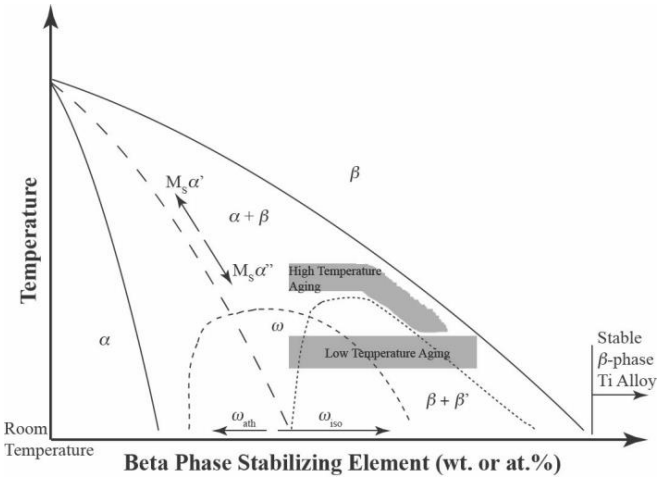

Figure 11. A schematic of a pseudo-binary isomorphous phase diagram from Figure 2 illustrating the differences between high and low isothermal aging temperatures for beta Ti alloys.

High temperature aging is conducted at approximately between 85 °C (185 °F) and 195 °C (383 °F) below the quantity T_β for short durations normally <24 h [34]. Santhosh et al. list an approximate

range of between 450 °C (842 °F) and 650 °C (1202 °F) [124]. Secondary hcp α-phase precipitates, which is an equilibrium phase, form initially at the bcc β-phase and then intragranularly at longer aging times. Intermediate metastable phases, such as the brittle isothermal ω-phase (ω_{iso}) or the β'-phase, usually do not form during high temperature aging. In general the size and volume fraction of α–phase precipitates depends on the alloy's composition and time at temperature. Higher aging temperatures and longer aging times form coarser α-phase precipitates leading to lower tensile strengths. For example, the near-beta Ti-10V-2Fe-3Al (wt. %) alloy has decreasing tensile strengths with increasing aging temperature between approximately 490 °C (914 °F) and 600 °C (1112 °F), Figure 12. Since the mechanical properties of beta Ti alloys can be optimized for an application by aging, numerous studies of the structure–property relationships are present in the existing literature [68,70,127,129,130]. These studies typically focus on microstructural evolution of the secondary α-phase precipitates and concomitant changes in tensile or hardness properties.

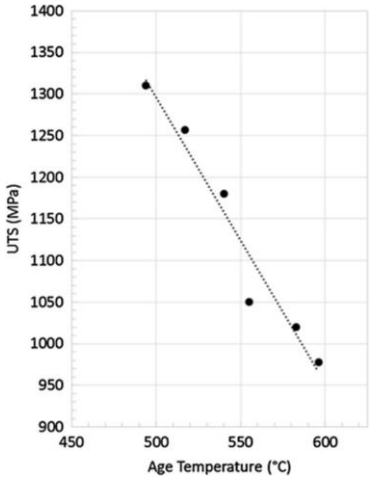

Figure 12. Ultimate tensile strength (UTS) as a function of aging temperature for the near-beta Ti-10V-2Fe-3Al (wt. %) alloy. The alloy was solution-treated at 750 °C (1385 °F) for 8 h, water-quenched and then isothermally aged [106]. (Reprinted by permission from Metallurgical Transaction A, vol. 18, no. 12, R. R. Boyer and G. W. Kuhlman, Processing properties relationships of Ti-10V-2Fe-3Al, 2095–2103, 1987, with permission from Springer Nature).

Low-temperature aging is typically conducted at approximately between 200 °C (392 °F) and 450 °C (842 °F) [34,124]. In this temperature range intermediate metastable phases such as the isothermal ω–phase or the β'–phase may form before the equilibrium hcp α-phase. The sequence of precipitation depends on whether the beta Ti alloy has a lower MoE value (solute lean) or a higher MoE Value (solute rich). In general the sequence of phase decomposition for alloys with lower MoE values such a the near-beta Ti-10V-2Fe-3Al (wt. %) alloy is

$$\beta \rightarrow \beta + \omega_{iso} \rightarrow \beta + \omega_{iso} + \alpha \rightarrow \beta + \alpha, \tag{3}$$

and for alloys with higher MoE value such as Ti-13V-11Cr-3Al (wt. %) is

$$\beta \rightarrow \beta + \beta' \rightarrow \beta + \beta' + \alpha \rightarrow \beta + \alpha \tag{4}$$

The low temperatures lead to very long aging times to complete the transformation to the equilibrium phases. The isothermal ω-phase precipitates found in Equation (3) causes embrittlement of the alloy [47] and thus the subject of numerous research articles, as discussed below. The coherent isothermal ω-phase precipitates are sheared during deformation, causing strong localized slip and pre-mature fracture with little or no ductility [124]. In the case of alloys with higher MoE values the bcc β-phase exhibits phase separation into the solute-rich β-phase and solute-lean β'-phase. These

metastable phases serve as heterogeneous nucleation sites for the equilibrium hcp α-phase. Studies are present in the existing literature on microstructural evolution of the secondary α-phase precipitates and concomitant changes in tensile or hardness properties during low temperature aging [69,131]. However, recent interest on the nucleation and growth mechanisms of the secondary α-phase precipitates in Equation (3) has made this the subject of several recent and detailed investigations. Li et al., have recently shown that the phase transformation process in a new Ti-6Cr-5Mo-5V-4Al (wt. %) alloy occurs at the bcc β-phase/isothermal ω-phase heterophase interfaces [132–134], These authors have proposed a mechanism where embryonic ω-phase, which forms initially by lattice plane displacement along the <111> direction, rapidly transforms to isothermal ω-phase precipitates through diffusion and depletion of O atoms, Figure 13. The O-rich region near the heterophase interfaces serves as nucleation sites for the secondary α-phase precipitates. Growth of the α-phase precipitates is a diffusive-displacement process that occurs through lattice reconstruction and diffusion and concurrent partitioning of Al, Mo, V, and Cr between the α-phase precipitates and β-phase matrix. Similar observations were recently made in the near-beta Ti-5Al-5Mo-5V-3Cr (wt. %) alloy [135,136] and the near-beta Ti-7Mo-3Nb-3Cr-3Al (wt. %) alloy [137]. The bcc β-phase to embryonic ω-phase transformation was recently clarified to occur through a displacive-diffusional process [138–140]. These authors demonstrated that the formation of ω-phase-like embryos occurred through competing compositional and structural instabilities arising in the bcc lattice of model binary Ti-Mo alloys during rapid cooling from the high-temperature single β-phase field. The transformation is initiated through the partial collapse of the {111} planes of the parent bcc structure and partitioning of Mo leading to its depletion in the ω-phase and enrichment in the β-phase matrix, Figure 14a–e. Less information is available in the existing literature about the phase transformation in Equation (4).

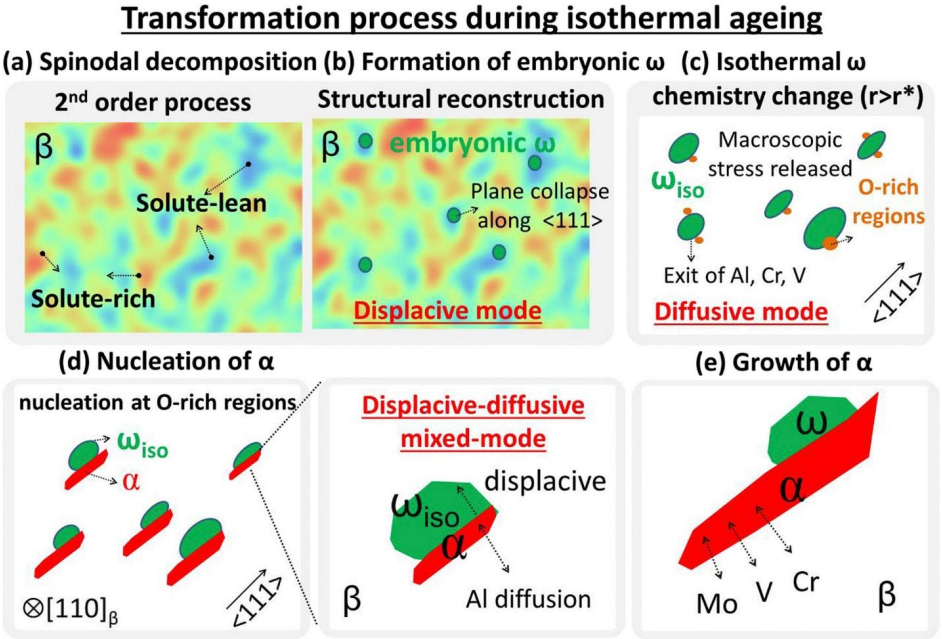

Figure 13. The phase transformation pathway from embryonic ω-phase, to isothermal ω-phase, to secondary α-phase precipitates during isothermal aging is illustrated [132]. (**a**) 2nd order coherent β-phase spinodal decomposition, (**b**) ω-phase embryos forms within certain composition range, where the structural evolution of embryonic ω-phase involves the displacement along the <111> direction, (**c**) when the size of embryonic ω-phase reaches a critical value, transformation from embryonic to isothermal ω-phase occurs via a diffusive mode, (**d**) O-rich regions present at the interface between isothermal ω-phase and β-phase matrix act as nucleation sites for α-phase, the transformation from ω-phase to α-phase involves lattice reconstruction as well as the diffusion of Al, (**e**) as the α-phase grows, the diffusion of Mo, V and Cr increases between α-phase and β-phase matrix. (Reprinted with permission from Acta Materialia, vol. 106, no. 12, T. Li et al., New insights into the phase transformations to isothermal ω and ω-assisted α in near β-Ti alloys, 353–366, 2016).

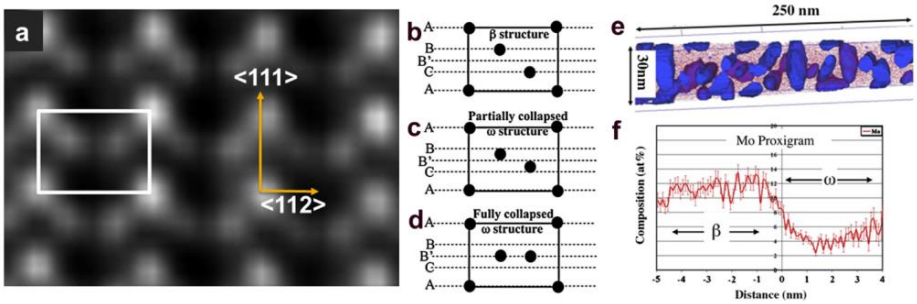

Figure 14. (**a**) The HAADF STEM image of fully transformed ω-phase in a model binary Ti-9 at. % Mo alloy [138]. (**b**–**d**) show the sequence of collapse of {111} planes of the bcc beta matrix to form ω-phase embryos. (**e**) shows the atom probe tomography (APT) reconstruction and (**f**) is the corresponding proximity histogram Mo concentration profile across the β-phase and ω-phase showing the Mo depleted ω-phase regions in the bcc beta phase matrix. (Reprinted with permission from Acta Materialia, vol. 60, A. Devaraj et al., Experimental evidence of concurrent compositional and structural instabilities leading to ω precipitation in titanium-molybdenum alloys, 596–609, 2012).

Recently, several articles have been published employing an innovative in situ high energy X-ray diffraction (HEXRD) technique on two commercially important beta Ti alloys. Barriobero-Vila et al., have used this technique to study the effect of constant heating rates after solution treatment to gain further insight into phase transformations kinetics and formation of the equilibrium α-phase in the near-beta Ti-10V-2Fe-3Al (wt. %) alloy [141] and the near-beta Ti-5Al-5Mo-5V-3Cr-1Zr (wt. %) alloy [142]. In the case of the Ti-10V-2Fe-3Al (wt. %) alloy [141], the initial microstructure after super-transus solution treatment consists of metastable athermal ω-phase particles and orthorhombic α''–martensite phase in a β-phase matrix. The authors illustrate that the α''-martensite phase reverts to the β-phase and the magnitude depends on the heating rate. Further, they show that at temperatures between approximately 420 °C (788 °F) and 650 °C (1202 °F) the stable α-phase forms by one of three mechanisms: (i) from α''-martensite phase plates, (ii) from isothermal α''-martensite phase that previously formed for the ω-phase, and (iii) from decomposition of the metastable β-phase. Similar experiments showed that in the Ti-5Al-5Mo-5V-3Cr-1Zr (wt. %) alloy [142], initial microstructure consists of athermal ω-phase particles along dislocation lines and in domains associated with decomposition of the β-phase matrix. For this alloy, the stable α-phase forms at temperatures between approximately 600 °C (1112 °F) and 650 °C (1202 °F) by decomposition of the β-phase and heterogeneous nucleation at grain boundaries or by transformation of the isothermal α''-martensite phase.

Duplex or two-step aging is performed to control the size and distribution of the secondary α-phase precipitates. The sequence is usually low temperature aging followed by high temperature aging for short times [34,124]. The actual temperatures and times chosen for the two steps must be optimized for an alloy's composition. Depending on the MoE value, a homogenous distribution of either the isothermal ω-phase or the solute-lean β'-phase will form during the first step. The main advantage of duplex aging is that the overall aging time is reduced compared to isothermal aging. This aging method may be used to improve thermal stability for elevated temperature applications, such as the Ti-15Mo-3Al-3Nb-0.2Si (wt. %) or B21S alloy [21]. The duplex aging method has been reported to promote a greater volume fraction of homogeneously distributed α-phase precipitates leading to improved alloy response under unidirectional tensile and fatigue loading conditions [124]. Furuhara et al., reported a more uniform and finer dispersion of α-phase precipitates after duplex aging, compared to isothermal aging [143]. These authors also reported that duplex aging resulted in higher hardness values due to faster precipitation kinetics. A good balance of strength and ductility was shown due to a finer and more uniform α-phase precipitation in the Ti-15V-3Al-3Cr-3Sn (wt. %) alloy [128]. Duplex aging resulted in superior fatigue limits and a slightly better fatigue crack growth behavior compared to direct aging in a metastable Ti-3Al-8V-6Cr-4Mo-4Zr (wt. %) alloy [144]. This was

attributed to the formation of homogeneously distributed α-phase precipitates and a lower volume fraction of grain boundary precipitates. In addition, the strength and percent elongation and reduction in area were better than for the isothermally aged alloys. Two-step aging of the Ti-15V-3Al-3Cr-3Sn (wt. %) alloy by Santhosh et al., led to higher strengths and hardness compared to isothermal aging, which was caused by a finer dispersion and higher number density of α-phase precipitates [145]. The authors also demonstrated that duplex aging of this alloy led to a four or five times increase of the high cycle fatigue strength [146]. Coakley et al., reported a qualitatively similar increase in hardness after duplex aging in the commercially important Ti-5Al-5Mo-5V-3Cr (wt. %) alloy [147]. It is clear that duplex aging can provide beneficial improvements for mechanical properties in some alloys.

Direct aging is when the beta Ti alloy is aged without prior solution treatment [34]. In general, this is performed when after the alloy has been cold worked. This process can hinder the formation of the deleterious isothermal ω-phase and homogeneous distribution of secondary hcp α-phase precipitates. However, the heat treatment must be optimized for an alloy's specific composition.

5. Stress-Induced Transformations

One important characteristic of these alloys is that the β-phase stability, which is a function of its composition, influences the deformation mechanisms during tensile, compressive, or creep loading. Deformation occurs by conventional viscous slip and stress-induced transformations, which are the hcp α'-martensite phase, the orthorhombic α''-martensite phase, the hexagonal ω-phase, and deformation twinning [33]. The formation of a specific stress-induced mechanism or mechanisms depends on the β-phase stability and influences the mechanical response and many studies are found in the existing literature on model binary, model ternary, and commercial beta Ti alloys [44,148–158]. The activity of these four deformation mechanisms are a function of the β-phase stability as quantified by MoE value and the microstructure or more specifically which metastable phases are present after thermo-mechanical processing and heat treatment. The general trend is for the martensitic phases to form in beta Ti alloys with lower MoE values during deformation, and the stress-induced deformation mechanism changes to the ω-phase and {332}<113> or {112}<111> twins as the MoE values and thus phase stability increases, Figure 15. In general, as the MoE value increases, the stress-induced deformation mechanisms follow the sequence of α'-martensite $\rightarrow$ α''-martensite $\rightarrow$ ω-phase + twinning $\rightarrow$ twinning $\rightarrow$ twinning + slip $\rightarrow$ slip. There is, however, a degree of overlap between the mechanisms since grain size, the presence or lack of a metastable phase, can promote or suppress a particular stress-induced deformation mechanism. The stress-induced transformations are suppressed when the bcc β-phase is stable and deformation by slip and eventually shear bands becomes the dominant mechanism. Additionally, the presence of metastable martensite phases or the ω-phase in the microstructure after heat treatment will serve as nucleation sites for stress-induced transformations during deformation. More than one stress-induced deformation mechanism and slip may also occur depending on the alloy's specific composition and β-phase stability.

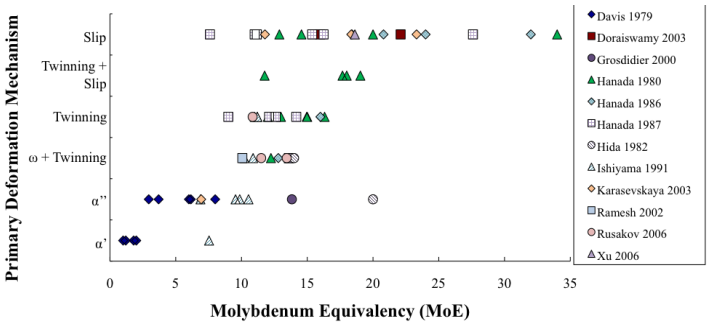

Figure 15. The experimental results that were reported for stress-induced deformation mechanisms as a function of MoE value for a broad range of beta Ti alloy compositions, microstructures, and mechanical property test methods [33]. (Reprinted with permission from JOM, vol. 67, no. 6, R. P. Kolli et al., Phase Stability and Stress-Induced Transformations in Beta Titanium Alloys, 1273–1280, 2015).

An alternate method to describe the occurrence of stress-induced transformations in beta Ti alloys is the phase stability diagram based on the mean *d*-orbital energy level, $\overline{M}_d$, and the mean bond order, $\overline{B}_o$ (referred to as the Bo vs. Md map) [12]:

$$\overline{M}_d = \sum_{i=1}^{n} x_i (M_d)_i \quad (5)$$

and

$$\overline{B}_o = \sum_{i=1}^{n} x_i (B_o)_i \quad (6)$$

where x_i is the atomic fraction of element i in the alloy, $(M_d)_i$ is the d-orbital energy level of element i, and $(B_o)_i$ is the bond order for element i, Figure 16. The quantity $(M_d)_i$ correlates to electronegativity and metallic radius of element i, whereas the quantity $(B_o)_i$ is a measure of the covalent bond strength between Ti and an alloying element. In general, the relationship between β-phase stability and MoE value and the quantities $\overline{M}_d$ and $\overline{B}_o$ is that the β-phase stability increases as the MoE value increases while the mean *d*-orbital energy level and the mean bond order decreases. Values for these three quantities correspond to the occurrence of specific stress-induced transformations. The formation of a specific type of stress-induced deformation mechanism is, however, more strongly dependent on the mean *d*-orbital energy level than the mean bond order. The relationship between the MoE value and the phase stability diagram occurs because many of the beta stabilizing elements have similar 3d or 4s orbital electron configurations and comparatively low electronegativities and atomic radii.

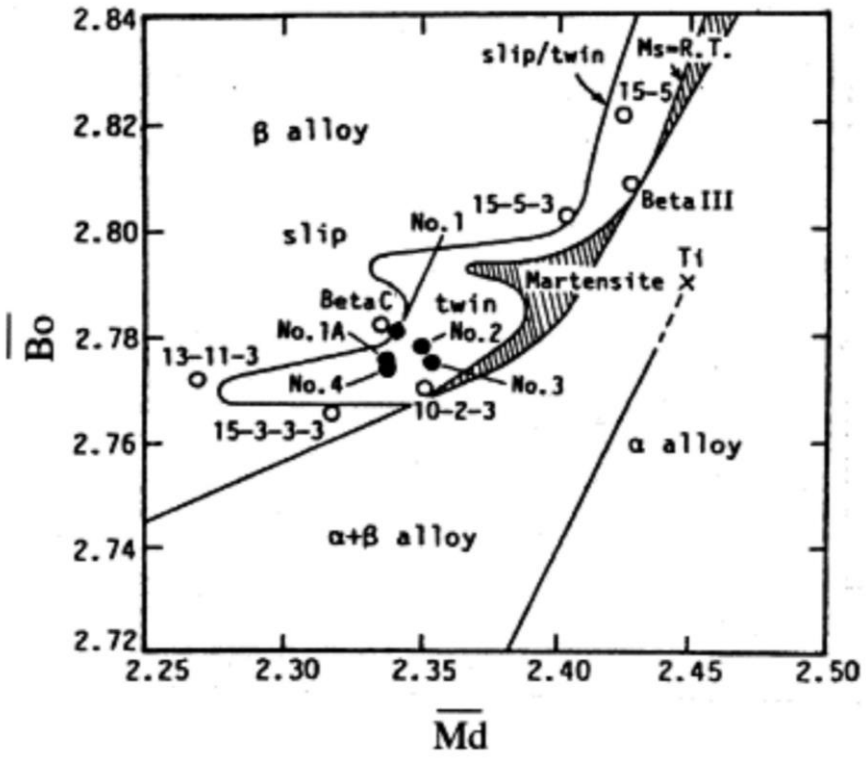

Figure 16. Phase-stability diagram for metastable and near-beta Ti alloys based on the mean *d*-orbital energy level, $\overline{M}_d$, and the mean bond order, $\overline{B}_o$ [12] (Reprinted with permission from Materials Science and Engineering A, vol. A243, D. Kuroda et al., Design and mechanical properties of new β type titanium alloys for implant materials, 244–249, 1998).

Research on stress-induced transformations is currently an active area of research due to its effect on mechanical response during deformation and its potential influence in engineering

applications [24,112,159–163]. A detailed review on this topic alone as provided by Kolli et al. [33]. Recently, an important work by Ahmed et al., studied the influence of β-phase stability on the deformation mechanisms in the metastable Ti-10V-3Fe-3Al (wt. %) alloy, which has a MoE of 12.4, during compressive loading after varying heat treatments [163]. They illustrated that {332}<113> twinning with α''-martensite, ω-phase, and slip were operational in the least stable alloy. Both {332}<113> twinning and {112}<111> twinning occurred with α''-martensite, ω-phase, and slip at intermediate stabilities. As the β-phase stability increased further {332}<113> twinning was no longer observed. Only dislocation glide (slip) was observed in the stable alloy. This is consistent with the trends in Figure 15. The same alloy was studied by Samiee et al., but during compression at a sub-transus temperature of 780 °C (1436 °F) [112]. These authors observed both stress-induced α''-martensite and ω-phase for the first time during deformation in the α + β phase field. Further, they measured that the volume fraction of α''-martensite was greater at the higher temperature than at ambient (room) temperature due to greater strains. They did not, however, observe twinning, which they attributed to the ease of slip at higher temperatures. Ahmed et al., also plotted their recent experimental results on the Bo vs. Md map. By including their and other recent results for Ti-10V-2Fe-3Al (wt. %), Ti-10V-2Cr-3Al (wt. %), and Ti-10V-1Fe-3Al (wt. %), these authors were able to show that the stress-induced martensite region is possibly larger than in the original diagram shown in Figure 16. Hence, they have proposed an expansion of the stress-induced martensite region on the lower part of the diagram, Figure 17, as indicated by the dashed blue line. Other authors have also recently proposed modifying the Bo vs. Md map. Barriobera-Vila et al., have recently studied the Ti-5Al-5V-5Mo-3Cr (wt. %) alloy to determine the sequence of stress-induced deformation mechanisms by an innovative in situ HEXRD under uniaxial compression technique [164]. They proposed to extend the martensite and slip boundaries based on their experimental characterization. These authors observed that both stress-induced martensite and slip can simultaneously occur although the alloy remains in the α + β phase field. However, the proposed changes need further investigation to determine the exact boundaries in the phase stability diagram and this is an area of research that needs to be addressed.

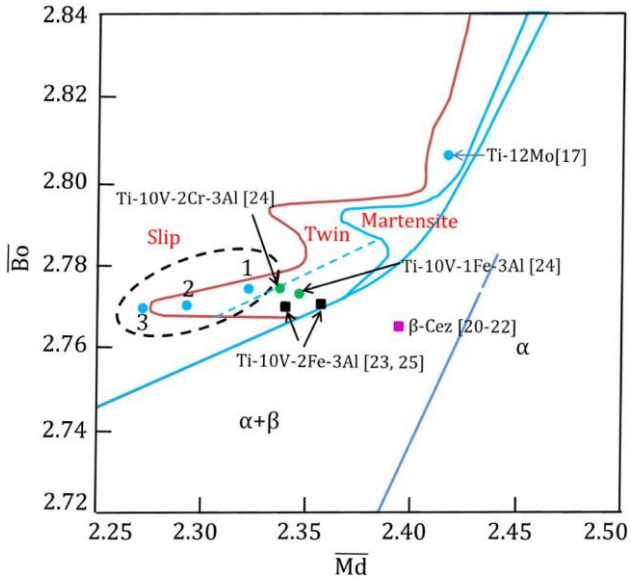

Figure 17. The proposed modified phase stability diagram for metastable and near-beta Ti alloys [163]. (Reprinted with permission from Acta Materialia, vol. 84, Ahmed et al., The influence of β phase stability on deformation mode and compressive mechanical properties of Ti-10V-3Fe-3Al alloy, 124–135, 2015).

One important effect of stress-induced deformation is the occurrence of room temperature superelastic behavior that occurs during the metastable β-phase to orthorhombic α''-martensite transformation. The superelastic effect occurs since this transformation is reversible. This has led to application of beta Ti alloys exhibiting this property in orthodontic arch wires, orthopedic bone plates, and stents. The most important commercial alloys are the Ti-Nb alloy system [56,165], and the Ti-23Nb-0.7Ta-2Zr (wt. %) alloy known as TNTZ alloy and the Ti-23Nb-0.7Ta-2Zr-1.2O (wt. %) alloy known as TNTZ-O alloy or "gum metal" [159]. In addition, a few Ti-Mo alloys have reportedly exhibited room-temperature superelasticity [61,152,159]. The superelastic effect is the subject of intense research owing to that fact that the exact mechanism is still the subject of debate and in some cases different studies contradict each other. Castany et al., employed a novel in situ cyclic tensile test under synchrotron X-ray diffraction method and investigated the metastable β-phase to orthorhombic α''-martensite transformation in detail for Ti-24Nb-0.5N (wt. %) and Ti-24Nb-0.5O (wt. %) alloys [166]. The element O is shown to more strongly influence the transformation behavior than the element N. Besse et al. [159] points out that in the case of the TNTZ and TNTZ-O alloys other mechanisms have been observed including dislocations, stress-induced {112}<111> or {332}<113> twins, and ω-phase plates and their role in superelastic behavior is not fully understood. However, stress-induced ω-phase was observed in binary Ti-Nb alloys and higher critical stress for slip deformation resulted in a larger recovery strain and stable superelasticity [165], which suggests that this phase improves superelastic properties.

Other areas of significant research include improving the superelastic behavior of Ti-Nb alloys. In general, these alloys have small recovery strains, which is due to the low critical stress for plastic deformation and the small transformation strain of stress-induced martensitic transformation. Several strategies are being actively researched including the effect of alloying elements, heat treatment, and texture control. The effect of alloying elements such as Sn on stress hysteresis, recovery strain, and superelastic properties was recently examined [167]. Increasing Sn concentrations were found to decrease the stress hysteresis but concomitantly increase the recovery strain. In addition, Sn suppresses the formation of athermal ω-phase and decreases the Ms temperatures reducing the stress for martensitic stress-induced martensite formation. Other research has illustrated that the addition of Zr and small quantities of Sn or Mo with controlled heat treatment to modify the texture and grain size increases recovery strain to ~7% and leads to excellent superelastic properties [168–173]. Further work is required to more fully understand superelasticity in these alloys. However, the small length scale and time scale of stress-induced transformations requires the use of in situ methods to more fully elucidate mechanisms.

6. Additive Manufacturing

Metal additive manufacturing (AM) has been the subject of recent intense research for numerous alloy systems including Ti alloys [174]. Most research on Ti alloys has been focused in optimizing powder feed stock and processing conditions, particularly for Ti-6Al-4V (wt. %) and a few other commercial alloys. Limited research is present in the existing literature about AM processing of metastable beta Ti alloys but a few recent studies have been reported using electron beam (e-beam) melting (EBM) [175–179] and selective laser melting (SLM) [177,180–182]. Much of this research has been focused on optimizing processing conditions or evaluating processing-structure-property relationships of Ti-24Nb-4Zr-8Sn (wt. %) alloys also known as Ti2448 alloy [175–180]. This alloy was developed for use in biomedical implants owing to its low modulus of elasticity and lack of elements with known toxicity in the human body. Although the Ti2448 alloy has low modulus of elasticity of approximately between 42 GPa and 50 GPa, this is, however, greater than cortical bone and may still cause stress shielding by an implant. One important aspect of this research is the development of high-strength-to-elastic modulus scaffolds. Scaffolds may lower the elastic modulus further still approaching that of cortical bone. However, the presence of Sn, which may vaporize and cause the formation of defects, e.g., porosity, leads to poor tensile and fatigue properties, Figure 18. Furthermore,

research on this alloy illustrated that EBM and SLM require different optimization and do not result in the same microstructure or properties. This example illustrates the difficulty of adapting existing beta Ti alloys to metal AM processing. The ability to tune mechanical properties based on phase volume fraction and composition was also illustrated for Ti-Nb alloys [181]. Much is still unknown about metastable beta Ti alloys processed by metal AM and this topic is anticipated to be one of significant research effort in the future. Further research is required to gain an increased understanding of the processing-structure-property relationships in metal AM. The application of metastable beta Ti alloys processed by AM is currently hindered due to limited knowledge about the microstructure and properties. The rapid cyclical heating and cooling that occurs during AM results in non-equilibrium microstructures or bulk defects that may not have the same properties as conventional wrought alloys of the same composition. Detailed experimental characterization is required to develop sufficient understanding of an alloy's processing characteristics and behavior in an application.

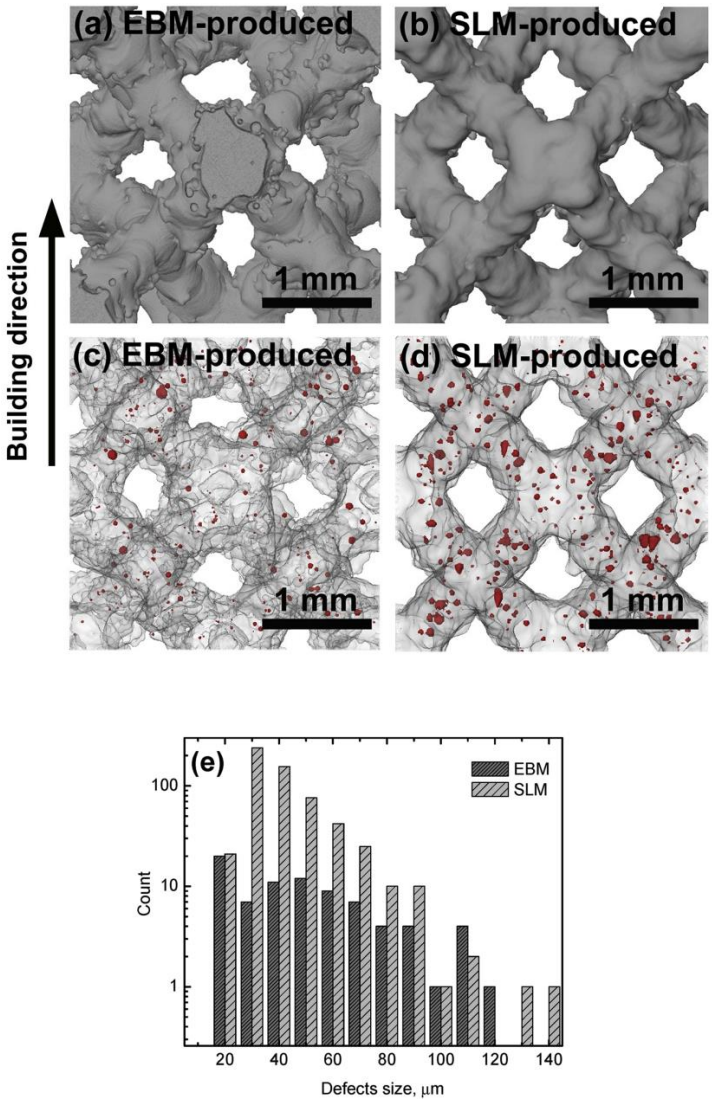

Figure 18. The micro-CT reconstructed images showing the strut outside surface of the (**a**) EBM and (**b**) SLM samples, the defects inside of the solid struts of the (**c**) EBM and (**d**) SLM samples, and (**e**) the size and count distribution of the defects inside the samples as a function of equivalent diameter [177]. (Reprinted with permission from Acta Materialia, vol. 113, Liu et al., Microstructure, defects and mechanical behavior of beta-type titanium porous structures manufactured by electron beam melting and selective laser melting, 56–67, 2016).

7. Summary

Beta titanium alloys are an important class of alloys that have found use in demanding applications such as aircraft structures and engines, and orthopedic and orthodontic implants. The advantages of these alloys include their high strength, good corrosion resistance, excellent biocompatibility, and ease of fabrication compared to other high performance alloys. The ease of fabrication, which is due to their lower beta transus temperature, provides these alloys with an advantage compared to other Ti alloy classes. The most important commercial beta Ti alloys for use in aircraft applications is the near-beta 10V-2Fe-3Al (wt. %) alloy, the metastable Ti-15Mo-3Cr-3Al-3Sn (wt. %) or B21S alloy, the Ti-3Al-8V-6Cr-4Mo-4Zr (wt. %) or Beta C alloy, the near-beta Ti-5Al-5Mo-5V-3Cr (wt. %) alloy, and the stable Ti-35V-15Cr (wt. %) or Alloy C. The most important commercial and experimental beta Ti alloys for use in orthopedic implants are the Ti-29Nb-13Ta-4.6Zr (wt. %) alloy and the Ti-13Nb-13Zr (wt. %) alloy. The mechanical properties and microstructure of these alloys are typically optimized by thermo-mechanical processing followed by solution treatment and aging process. The metastable bcc β-phase decomposes to form equilibrium hcp α-phase precipitates. Intermediate metastable phases, such as the isothermal ω-phase, form first and serve as heterogeneous nucleation sites for the equilibrium α-phase. Despite their advantages and promise, beta Ti alloys have only found use in niche applications due to their high costs associated with extraction, processing, and alloying. As discussed above, extraction is a complex and costly process and progress in lowering the cost is often incremental. Further, many of the alloying elements are expensive refractory ones, e.g., Mo, V, and Nb, although in the case of biomedical implants they may provide benefits of lower toxicity and improved biocompatibility. Beta Ti alloys also possess higher densities than other classes of Ti alloys due to high concentrations of beta stabilizing elements, which is a disadvantage when low mass is a requirement. However, the improved and tunable mechanical properties may lead to good specific strength and specific modulus values for a desired application. In addition, several other challenges exist in that they generally have more complex and narrower thermo-mechanical processing and heat treatment windows than other Ti alloys and high-performance alloys, higher machining costs, lower production volumes, and less readily available property data. New beta Ti alloys should address some of the aforesaid deficiencies in order to achieve commercial success in aerospace structures and biomedical implant applications.

From a manufacturing perspective, research on thermo-mechanical processing and heat treatment are expected to increase, particularly for current commercially important and newly developed beta Ti alloys. Altering the processing or solutionizing temperature between super-transus and sub-transus temperatures results in significant changes to microstructure and concomitantly to properties. This high degree of sensitivity can lead to tunable mechanical properties for a desired application. The important ability to alter the modulus to low values approaching that of cortical bone will also promote further research. A second important property is the superelastic behavior resulting from stress-induced orthorhombic α''-martensite phase. However, as discussed above, this phase may lead to unsatisfactory mechanical behavior through reduced ductility and stress inhomogeneity limiting its use in structural applications. Further research on processing and heat treatment of alloys exhibiting room temperature superelastic behavior is required to gain improved understanding of its effect on mechanical response. A third area that is exhibiting significant growth in research is processing by metal AM. Since this process consists of repeated and rapid heating and cooling cycles in a layer-by-layer deposition of metal, the resulting microstructure is not at equilibrium. The as deposited microstructure and the effect of post-processing heat treatment are largely unknown for many beta Ti alloys.

In terms of fundamental scientific understanding, research effort on beta Ti alloys is increasing significantly, Figure 19. The historical number of peer-reviewed scientific publications on metastable beta titanium alloys has now reached approximately 650. The historic trend of number of publications shows very limited research before 1960, then an increased activity of research from ~1970 to mid-1980s during the development of several commercial alloys for use in aircraft and orthopedic and orthodontic implants. Since 1990 to 2017, the number of publications has

experienced significant growth. This number is anticipated to grow further as new alloys are developed and advanced characterization tools and computational techniques permit elucidation of processing–structure–property relationships. Several areas merit further study, including the role of the β'-phase during nucleation of the equilibrium α-phase, the effect of O interstitial atoms on stress-induced deformation mechanisms, thermo-mechanical processing and heat treatment of newly developed alloys, stress-induced transformation at temperatures above ambient (room) temperature, processing by metal AM, and developing new beta Ti alloys that address some of the aforesaid limitations for commercial applications.

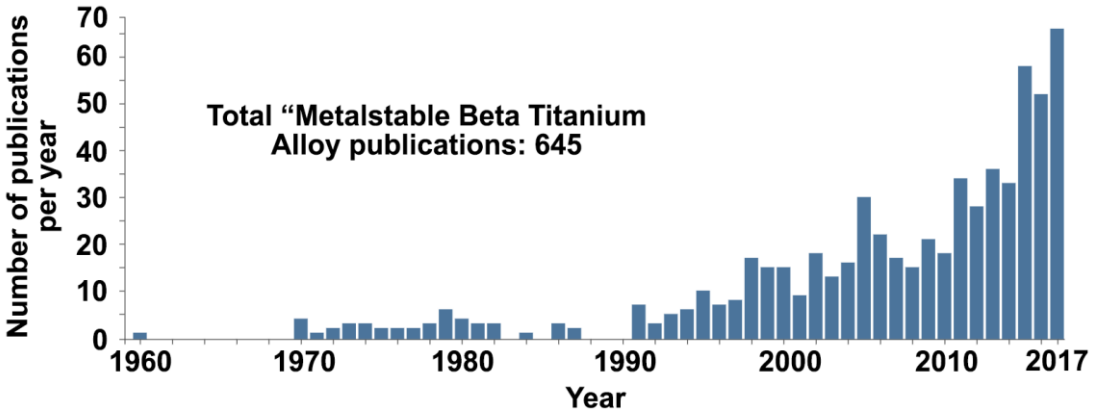

Figure 19. History of number of publications on "Metastable beta titanium alloy" from Web of Science.

An improved scientific understanding of the processing–structure–property relationships is hindered by the small length-scale of the metastable phases and stress-induced transformations of beta Ti alloys. However, some length-scale challenges can be addressed by employing state-of-the-art techniques such as atom probe tomography (APT) [183], high-resolution transmission electron microscopy (HRTEM), and high-angle annular dark-field imaging in scanning transmission electron microscope mode (HAADF-STEM). The use of complementary APT experimental techniques such as APT with HAADF-STEM can provide a combination of nano-scale compositional and structural information that one technique alone cannot provide possibly leading to greater scientific understanding [184]. A recent important example is the study by Ahmed et al., who employed complementary APT with HAADF-STEM imaging to illuminate phase decomposition of the Ti-5Al-5Mo-5V-2Cr-1Fe (wt. %) alloy during aging [130]. These authors were able to illustrate the early stages of β-phase decomposition and isothermal α-phase nucleation and growth that is generally not accessible by one technique. Similarly, complementary APT techniques combining experimental characterization with computational methods such as Calculation of Phase Diagrams (CALPHAD) may provide improved understanding of the metastable transformations in these alloys. There are, however, several challenges for employing computational methods. In context of CALPHAD, thermodynamic databases for Ti alloys exist but may need to be modified for study of beta Ti alloys. In addition, study of diffusion kinetics and precipitation during aging are limited by the absence of suitable mobility databases. Another challenge is the short time-scale of many phase and stress-induced transformations that often makes experimental observations and measurements very difficult. However, in situ transmission electron microscopy (TEM) observations or in situ synchrotron X-ray diffraction (XRD)-based techniques may provide clarity for the early stages of phase transformation. In some cases, in situ TEM may lack the requisite resolution to observe the transformations. But advances in micro-electrical-mechanical-systems (MEMS) devices that can act as specimen holders have facilitated the ability to locally control specimen environment making these types of experiments easier to conduct. Synchrotron studies provide greater resolution and a high-energy source but access is often difficult. Furthermore, first principles calculations are suitable

to provide complementary analysis of in situ studies. However, they are computationally expensive and are often limited to the study of model binary alloys.

Author Contributions: Both R.P.K. and A.D. wrote this review article.

Funding: No funding was received for writing this review article.

Acknowledgments: A.D. would like to acknowledge Physical and Computational Science Directorate seed funding from Laboratory Directed Research and development program.

Conflicts of Interest: The authors declare no conflict of interest.

References

1. Banerjee, D.; Williams, J.C. Perspectives on Titanium Science and Technology. *Acta Mater.* **2013**, *61*, 844–879. [CrossRef]
2. Lütjering, G.; Williams, J.C. *Titanium*, 2nd ed.; Springer: Berlin, Germany, 2007; ISBN 978-3-540-73036-1.
3. Boyer, R.R. An overview on the use of titanium in the aerospace industry. *Mater. Sci. Eng. A* **1996**, *213*, 103–114. [CrossRef]
4. Peters, M.; Kumpfert, J.; Ward, C.H.; Leyens, C. Titanium Alloys for Aerospace Applications. *Adv. Eng. Mater.* **2003**, *5*, 419–427. [CrossRef]
5. Leyens, C.; Peters, M. (Eds.) *Titanium and Titanium Alloys*; Wiley-VCH GmbH & Co.: Weinheim, Germany, 2006; ISBN 978-3-527-60520-0.
6. Niinomi, M. Recent research and development in titanium alloys for biomedical applications and healthcare goods. *Sci. Technol. Adv. Mater.* **2003**, *4*, 445. [CrossRef]
7. Niinomi, M. Recent metallic materials for biomedical applications. *Metall. Mater. Trans. A* **2002**, *33*, 477–486. [CrossRef]
8. Niinomi, M. Mechanical properties of biomedical titanium alloys. *Mater. Sci. Eng. A* **1998**, *243*, 231–236. [CrossRef]
9. Niinomi, M. Mechanical biocompatibilities of titanium alloys for biomedical applications. *J. Mech. Behav. Biomed.* **2008**, *1*, 30–42. [CrossRef] [PubMed]
10. Rack, H.J.; Qazi, J.I. Titanium alloys for biomedical applications. *Mater. Sci. Eng. C* **2006**, *26*, 1269–1277. [CrossRef]
11. Geetha, M.; Singh, A.K.; Asokamani, R.; Gogia, A.K. Ti based biomaterials, the ultimate choice for orthopaedic implants—A review. *Prog. Mater. Sci.* **2009**, *54*, 397–425. [CrossRef]
12. Kuroda, D.; Niinomi, M.; Morinaga, M.; Kato, Y.; Yashiro, T. Design and mechanical properties of new β type titanium alloys for implant materials. *Mater. Sci. Eng. A* **1998**, *243*, 244–249. [CrossRef]
13. Li, Y.; Yang, C.; Zhao, H.; Qu, S.; Li, X.; Li, Y. New Developments of Ti-Based Alloys for Biomedical Applications. *Materials* **2014**, *7*, 1709–1800. [CrossRef] [PubMed]
14. Schutz, R.W.; Watkins, H.B. Recent developments in titanium alloy application in the energy industry. *Mater. Sci. Eng. A* **1998**, *243*, 305–315. [CrossRef]
15. Cooper, S.P.; Whitley, G.H. Titanium in the power generation industry. *Mater. Sci. Technol.* **1987**, *3*, 91–96. [CrossRef]
16. Inagaki, I.; Shirai, Y.; Takechi, T.; Ariyasu, N. *Application and Features of Titanium for the Aerospace Industry*; Nippon Steel & Sumitomo Metal: Osaka City, Japan, 2014; pp. 22–27.
17. Welsch, G.; Boyer, R.; Collings, E.W. *Materials Properties Handbook: Titanium Alloys*; ASM International: Materials Park, OH, USA, 1994; ISBN 978-0-87170-481-8.
18. Nayak, S.K.; Hung, C.J.; Sharma, V.; Alpay, S.P.; Dongare, A.M.; Brindley, W.J.; Hebert, R.J. Insight into point defects and impurities in titanium from first principles. *Comput. Mater.* **2018**, *4*, 11. [CrossRef]
19. Wasz, M.L.; Brotzen, F.R.; McLellan, R.B.; Griffin, A.J. Effect of oxygen and hydrogen on mechanical properties of commercial purity titanium. *Int. Mater. Rev.* **1996**, *41*, 1–12. [CrossRef]
20. Brandes, M.C.; Baughman, M.; Mills, M.J.; Williams, J.C. The effect of oxygen and stress state on the yield behavior of commercially pure titanium. *Mater. Sci. Eng. A* **2012**, *551*, 13–18. [CrossRef]
21. Cotton, J.D.; Briggs, R.D.; Boyer, R.R.; Tamirisakandala, S.; Russo, P.; Shchetnikov, N.; Fanning, J.C. State of the Art in Beta Titanium Alloys for Airframe Applications. *JOM* **2015**, *67*, 1281–1303. [CrossRef]

22. Niinomi, M.; Hattori, T.; Morikawa, K.; Kasuga, T.; Suzuki, A.; Fukui, H.; Niwa, S. Development of Low Rigidity β-type Titanium Alloy for Biomedical Applications. *Mater. Trans.* **2002**, *43*, 2970–2977. [CrossRef]
23. Castro, S.M.; Ponces, M.J.; Lopes, J.D.; Vasconcelos, M.; Pollmann, M.C.F. Orthodontic wires and its corrosion—The specific case of stainless steel and beta-titanium. *J. Dent. Sci.* **2015**, *10*, 1–7. [CrossRef]
24. Gutierrez-Urrutia, I.; Li, C.-L.; Emura, S.; Min, X.; Tsuchiya, K. Study of 332<113> twinning in a multilayered Ti-10Mo-xFe (x = 1–3) alloy by ECCI and EBSD. *Sci. Technol. Adv. Mater.* **2016**, *17*, 220–228. [CrossRef] [PubMed]
25. Okulov, I.V.; Wendrock, H.; Volegov, A.S.; Attar, H.; Kuhn, U.; Skrotzki, W.; Eckert, J. High strength beta titanium alloys: New design approach. *Mater. Sci. Eng. A* **2015**, *628*, 297–302. [CrossRef]
26. Okulov, I.V.; Pauly, S.; Kuhn, U.; Gargarella, P.; Marr, T.; Freudenberger, J.; Schultz, L.; Scharnweber, J.; Oertel, C.-G.; Skrotzki, W.; et al. Effect of microstructure on the mechanical properties of as-cast Ti–Nb–Al–Cu–Ni alloys for biomedical application. *Mater. Sci. Eng. C* **2013**, *33*, 4795–4801. [CrossRef] [PubMed]
27. Sengupta, B.; Shekhar, S.; Kulkarni, K.N. A novel ultra-high strength and low-cost as-cast titanium alloy. *Mater. Sci. Eng. A* **2017**, *696*, 478–481. [CrossRef]
28. Imayev, V.M.; Gaisin, R.A.; Gaisina, E.R.; Imayev, R.M. Microstructure, processing and mechanical properties of a titanium alloy Ti-20Zr-6.5Al-3.3Mo-0.3Si-0.1B. *Mater. Sci. Eng. A* **2017**, *696*, 137–145. [CrossRef]
29. Zhao, G.-H.; Ketov, S.V.; Jiang, J.; Mao, H.; Borgenstam, A.; Louzguine-Luzgin, D.V. New beta-type Ti-Fe-Sn-Nb alloys with superior mechanical strength. *Mater. Sci. Eng. A* **2017**, *705*, 348–351. [CrossRef]
30. Kopova, I.; Strasky, J.; Harcuba, P.; Landa, M.; Janecek, M.; Bacakova, L. Newly developed Ti-Nb-Zr-Ta-Si-Fe biomedical beta titanium alloys with increased strength and enhanced biocompatibility. *Mater. Sci. Eng. C* **2016**, *60*, 230–238. [CrossRef] [PubMed]
31. Nnamchi, P.S.; Obayi, C.S.; Todd, I.; Rainforth, M.W. Mechanical and electrochemical characterisation of new Ti-Mo-Nb-Zr alloys for biomedical applications. *J. Mech. Behav. Biomed. Mater.* **2016**, *60*, 68–77. [CrossRef] [PubMed]
32. Hida, M.; Miyazawa, K.; Tsuruta, S.; Kurosawa, M.; Hata, Y.; Kawai, T.; Goto, S. Effect of heat treatment conditions on the mechanical properties of Ti-6Mo-4Sn alloy for orthodontic wires. *Dent. Mater. J.* **2013**, *32*, 462–467. [CrossRef] [PubMed]
33. Kolli, R.P.; Joost, W.J.; Ankem, S. Phase Stability and Stress-Induced Transformations in Beta Titanium Alloys. *JOM* **2015**, *67*, 1273–1280. [CrossRef]
34. Ankem, S.; Seagle, S.R. Heat Treatment of Metastable Beta Titanium Alloys. In *Beta Titanium Alloys in the 1980's*; Boyer, R.R., Rosenberg, H.W., Eds.; AIME: Warrendale, PA, USA, 1984; pp. 107–126.
35. Froes, F.H.; Bomberger, H.B. The Beta Titanium Alloys. *JOM* **1985**, *37*, 28–37. [CrossRef]
36. Bania, P.J. Beta titanium alloys and their role in the titanium industry. *JOM* **1994**, *46*, 16–19. [CrossRef]
37. Murray, J.L. *Phase Diagrams of Binary Titanium Alloys*; ASM International: Metals Park, OH, USA, 1987; ISBN 0-87170-248-7.
38. Murray, J.L. The Cr-Ti (chromium-titanium) system. *Bull. Alloy Phase Diagr.* **1981**, *2*, 174–181. [CrossRef]
39. Aiyangar, A.K.; Neuberger, B.W.; Oberson, P.G.; Ankem, S. The effects of stress level and grain size on the ambient temperature creep deformation behavior of an alpha Ti-1.6 wt pct V alloy. *Metall. Mater. Trans. A* **2005**, *36*, 637–644. [CrossRef]
40. Oberson, P.G.; Ankem, S. The effect of time-dependent twinning on low temperature (<0.25 * *T*m) creep of an alpha-titanium alloy. *Int. J. Plast.* **2009**, *25*, 881–900. [CrossRef]
41. Jaworski, A.; Ankem, S. The effect of α phase on the deformation mechanisms of β titanium alloys. *J. Mater. Eng. Perform.* **2005**, *14*, 755–760. [CrossRef]
42. Jaworski, A., Jr.; Ankem, S. Influence of the second phase on the room-temperature tensile and creep deformation mechanisms of α-β titanium alloys: Part I. Tensile deformation. *Metall. Mater. Trans. A* **2006**, *37*, 2739–2754. [CrossRef]
43. Jaworski, A., Jr.; Ankem, S. Influence of the second phase on the room-temperature tensile and creep deformation mechanisms of α-β titanium alloys, part II: Creep deformation. *Metall. Mater. Trans. A* **2006**, *37*, 2755–2765. [CrossRef]
44. Ramesh, A.; Ankem, S. The effect of grain size on the ambient temperature creep deformation behavior of a beta Ti-14.8 V alloy. *Metall. Mater. Trans. A* **2002**, *33*, 1137–1144. [CrossRef]

45. Davis, R.; Flower, H.M.; West, D.R.F. Martensitic transformations in Ti-Mo alloys. *J. Mater. Sci.* **1979**, *14*, 712–722. [CrossRef]
46. Menon, E.S.K.; Krishnan, R. Phase transformations in Ti-V alloys. *J. Mater. Sci.* **1983**, *18*, 365–374. [CrossRef]
47. Williams, J.C.; Hickman, B.S.; Marcus, H.L. The effect of omega phase on the mechanical properties of titanium alloys. *Metall. Trans.* **1971**, *2*, 1913–1919. [CrossRef]
48. Silcock, J.M. An X-ray examination of the to phase in TiV, TiMo and TiCr alloys. *Acta Metall.* **1958**, *6*, 481–493. [CrossRef]
49. De Fontaine, D.; Paton, N.E.; Williams, J.C. The omega phase transformation in titanium alloys as an example of displacement controlled reactions. *Acta Metall.* **1971**, *19*, 1153–1162. [CrossRef]
50. Banerjee, S.; Tewari, R.; Dey, G.K. Omega phase transformation-morphologies and mechanisms. *Int. J. Mater. Res.* **2006**, *97*, 963–977. [CrossRef]
51. Clément, N.; Lenain, A.; Jacques, P.J. Mechanical property optimization via microstructural control of new metastable beta titanium alloys. *JOM* **2007**, *59*, 50–53. [CrossRef]
52. Donachie, M.J. *Titanium: A Technical Guide*, 2nd ed.; ASM International: Materials Park, OH, USA, 2000; ISBN 978-1-61503-062-0.
53. Williams, J.C.; Hickman, B.S.; Leslie, D.H. The effect of ternary additions on the decompositon of metastable beta-phase titanium alloys. *Metall. Trans.* **1971**, *2*, 477–484. [CrossRef]
54. Joost, W.J.; Ankem, S.; Kuklja, M.M. A modified embedded atom method potential for the titanium–oxygen system. *Model. Simul. Mater. Sci. Eng.* **2015**, *23*, 015006. [CrossRef]
55. Obbard, E.G.; Hao, Y.L.; Talling, R.J.; Li, S.J.; Zhang, Y.W.; Dye, D.; Yang, R. The effect of oxygen on α'' martensite and superelasticity in Ti-24Nb-4Zr-8Sn. *Acta Mater.* **2011**, *59*, 112–125. [CrossRef]
56. Tahara, M.; Kim, H.Y.; Inamura, T.; Hosoda, H.; Miyazaki, S. Lattice modulation and superelasticity in oxygen-added β-Ti alloys. *Acta Mater.* **2011**, *59*, 6208–6218. [CrossRef]
57. Pang, E.L.; Pickering, E.J.; Baik, S.I.; Seidman, D.N.; Jones, N.G. The effect of zirconium on the omega phase in Ti-24Nb-[0–8]Zr (at. %) alloys. *Acta Mater.* **2018**, *153*, 62–70. [CrossRef]
58. Weiss, I.; Semiatin, S.L. Thermomechanical processing of beta titanium alloys—An overview. *Mater. Sci. Eng. A* **1998**, *243*, 46–65. [CrossRef]
59. Tiwari, G.P.; Ramanujan, R.V. Review The relation between the electron to atom ratio and some properties of metallic systems. *J. Mater. Sci.* **2001**, *36*, 271–283. [CrossRef]
60. Nyakana, S.L.; Fanning, J.C.; Boyer, R.R. Quick reference guide for β titanium alloys in the 00s. *J. Mater. Eng. Perform.* **2005**, *14*, 799–811. [CrossRef]
61. Grosdidier, T.; Roubaud, C.; Philippe, M.-J.; Combres, Y. The deformation mechanisms in the β-metastable β-Cez titanium alloy. *Scr. Mater.* **1997**, *36*, 21–28. [CrossRef]
62. Boyer, R.R.; Briggs, R.D. The use of β titanium alloys in the aerospace industry. *J. Mater. Eng. Perform.* **2005**, *14*, 681–685. [CrossRef]
63. Fanning, J.C. Properties of TIMETAL 555 (Ti-5Al-5Mo-5V-3Cr-0.6Fe). *J. Mater. Eng. Perform.* **2005**, *14*, 788–791. [CrossRef]
64. Fanning, J.C.; Fox, S.P. Recent developments in metastable β strip alloys. *J. Mater. Eng. Perform.* **2005**, *14*, 703–708. [CrossRef]
65. Fan, J.K.; Kou, H.C.; Lai, M.J.; Tang, H.; Chang, H.; Li, J.S. Characterization of hot deformation behavior of a new near beta titanium alloy: Ti-7333. *Mater. Des.* **2013**, *49*, 945–952. [CrossRef]
66. Hua, K.; Li, J.; Kou, H.; Fan, J.; Sun, M.; Tang, B. Phase precipitation behavior during isothermal deformation in β-quenched near beta titanium alloy Ti-7333. *J. Alloy Compd.* **2016**, *671*, 381–388. [CrossRef]
67. Wang, Z.; Wang, X.; Zhu, Z. Characterization of high-temperature deformation behavior and processing map of TB17 titanium alloy. *J. Alloy Compd.* **2017**, *692*, 149–154. [CrossRef]
68. Sadeghpour, S.; Abbasi, S.M.; Morakabati, M.; Bruschi, S. Correlation between alpha phase morphology and tensile properties of a new beta titanium alloy. *Mater. Des.* **2017**, *121*, 24–35. [CrossRef]
69. Du, Z.X.; Xiao, S.L.; Shen, Y.P.; Liu, J.S.; Liu, J.; Xu, L.J.; Kong, F.T.; Chen, Y.Y. Effect of hot rolling and heat treatment on microstructure and tensile properties of high strength beta titanium alloy sheets. *Mater. Sci. Eng. A* **2015**, *631*, 67–74. [CrossRef]
70. Du, Z.; Xiao, S.; Xu, L.; Tian, J.; Kong, F.; Chen, Y. Effect of heat treatment on microstructure and mechanical properties of a new β high strength titanium alloy. *Mater. Des.* **2014**, *55*, 183–190. [CrossRef]

71. Domingo, J.L. Vanadium: A review of the reproductive and developmental toxicity. *Reprod. Toxicol.* **1996**, *10*, 175–182. [CrossRef]
72. Bondy, S.C. The neurotoxicity of environmental aluminum is still an issue. *NeuroToxicology* **2010**, *31*, 575–581. [CrossRef] [PubMed]
73. Bondy, S.C. Low levels of aluminum can lead to behavioral and morphological changes associated with Alzheimer's disease and age-related neurodegeneration. *NeuroToxicology* **2016**, *52*, 222–229. [CrossRef] [PubMed]
74. Tsaryk, R.; Peters, K.; Barth, S.; Unger, R.E.; Scharnweber, D.; Kirkpatrick, C.J. The role of oxidative stress in pro-inflammatory activation of human endothelial cells on Ti6Al4V alloy. *Biomaterials* **2013**, *34*, 8075–8085. [CrossRef] [PubMed]
75. Eisenbarth, E.; Velten, D.; Muller, M.; Thull, R.; Breme, J. Biocompatibility of β-stabilizing elements of titanium alloys. *Biomaterials* **2004**, *25*, 5705–5713. [CrossRef] [PubMed]
76. Wang, K. The use of titanium for medical applications in the USA. *Mater. Sci. Eng. A* **1996**, *213*, 134–137. [CrossRef]
77. Pilliar, R.M.; Cameron, H.U.; Binnington, A.G.; Szivek, J.; Macnab, I. Bone ingrowth and stress shielding with a porous surface coated fracture fixation plate. *J. Biomed. Mater. Res.* **1979**, *13*, 799–810. [CrossRef] [PubMed]
78. Matsuno, H.; Yokoyama, A.; Watari, F.; Uo, M.; Kawasaki, T. Biocompatibility and osteogenesis of refractory metal implants, titanium, hafnium, niobium, tantalum and rhenium. *Biomaterials* **2001**, *22*, 1253–1262. [CrossRef]
79. Trentani, L.; Pelillo, F.; Pavesi, F.C.; Ceciliani, L.; Cetta, G.; Forlino, A. Evaluation of the TiMo12Zr6Fe2 alloy for orthopaedic implants: In vitro biocompatibility study by using primary human fibroblasts and osteoblasts. *Biomaterials* **2002**, *23*, 2863–2869. [CrossRef]
80. Nag, S.; Banerjee, R.; Fraser, H.L. Microstructural evolution and strengthening mechanisms in Ti-Nb-Zr-Ta, Ti-Mo-Zr-Fe and Ti-15Mo biocompatible alloys. *Mater. Sci. Eng. C* **2005**, *25*, 357–362. [CrossRef]
81. Nag, S.; Banerjee, R.; Fraser, H.L. Intra-granular alpha precipitation in Ti-Nb-Zr-Ta biomedical alloys. *J. Mater. Sci.* **2009**, *44*, 808–815. [CrossRef]
82. Guo, S.; Meng, Q.; Zhao, X.; Wei, Q.; Xu, H. Design and fabrication of a metastable β-type titanium alloy with ultralow elastic modulus and high strength. *Sci. Rep.* **2015**, *5*, 14688. [CrossRef] [PubMed]
83. Santos, P.F.; Niinomi, M.; Cho, K.; Nakai, M.; Liu, H.; Ohtsu, N.; Hirano, M.; Ikeda, M.; Narushima, T. Microstructures, mechanical properties and cytotoxicity of low cost beta Ti-Mn alloys for biomedical applications. *Acta Biomater.* **2015**, *26*, 366–376. [CrossRef] [PubMed]
84. Goldberg, J.; Burstone, C.J. An Evaluation of Beta Titanium Alloys for Use in Orthodontic Appliances. *J. Dent. Res.* **1979**, *58*, 593–599. [CrossRef] [PubMed]
85. Burstone, C.J.; Goldberg, A.J. Beta titanium: A new orthodontic alloy. *Am. J. Orthod.* **1980**, *77*, 121–132. [CrossRef]
86. Goldberg, A.J.; Shastry, C.V. Age hardening of orthodontic beta titanium alloys. *J. Biomed. Mater. Res.* **1984**, *18*, 155–163. [CrossRef]
87. Wilson, D.F.; Goldberg, A.J. Alternative beta-titanium alloys for orthodontic wires. *Dent. Mater.* **1987**, *3*, 337–341. [CrossRef]
88. Kaneko, K.; Yokoyama, K.; Moriyama, K.; Asaoka, K.; Sakai, J.; Nagumo, M. Delayed fracture of beta titanium orthodontic wire in fluoride aqueous solutions. *Biomaterials* **2003**, *24*, 2113–2120. [CrossRef]
89. Martins, R.P.; Caldas, S.G.F.R.; Ribeiro, A.A.; Vaz, L.G.; Shimizu, R.H.; Martins, L.P.; Martins, R.P.; Caldas, S.G.F.R.; Ribeiro, A.A.; Vaz, L.G.; et al. Differences in the force system delivered by different beta-titanium wires in elaborate designs. *Dent. Press J. Orthod.* **2015**, *20*, 89–96. [CrossRef] [PubMed]
90. Verstrynge, A.; Humbeeck, J.V.; Willems, G. In-vitro evaluation of the material characteristics of stainless steel and beta-titanium orthodontic wires. *Am. J. Orthod. Dentofac. Orthop.* **2006**, *130*, 460–470. [CrossRef] [PubMed]
91. Juvvadi, S.R.; Kailasam, V.; Padmanabhan, S.; Chitharanjan, A.B. Physical, mechanical, and flexural properties of 3 orthodontic wires: An in-vitro study. *Am. J. Orthod. Dentofac. Orthop.* **2010**, *138*, 623–630. [CrossRef] [PubMed]
92. Iijima, M.; Muguruma, T.; Brantley, W.A.; Mizoguchi, I. Comparisons of nanoindentation, 3-point bending, and tension tests for orthodontic wires. *Am. J. Orthod. Dentofac. Orthop.* **2011**, *140*, 65–71. [CrossRef] [PubMed]

93. Duraccio, D.; Mussano, F.; Faga, M.G. Biomaterials for dental implants: Current and future trends. *J. Mater. Sci.* **2015**, *50*, 4779–4812. [CrossRef]
94. Brånemark, P.-I.; Breine, U.; Adell, R.; Hansson, B.O.; Lindström, J.; Ohlsson, Å. Intra-Osseous Anchorage of Dental Prostheses:I. Experimental Studies. *Scand. J. Plast. Reconstr. Surg.* **1969**, *3*, 81–100. [CrossRef] [PubMed]
95. Adell, R.; Lekholm, U.; Rockler, B.; Brånemark, P.-I. A 15-year study of osseointegrated implants in the treatment of the edentulous jaw. *Int. J. Oral Surg.* **1981**, *10*, 387–416. [CrossRef]
96. Adell, R.; Eriksson, B.; Lekholm, U.; Brånemark, P.I.; Jemt, T. Long-term follow-up study of osseointegrated implants in the treatment of totally edentulous jaws. *Int. J. Oral Maxillofac. Implants* **1990**, *5*, 347–359. [PubMed]
97. Milošev, I.; Hmeljak, J.; Žerjav, G.; Cör, A.; Moreno, J.M.C.; Popa, M. Quaternary Ti-20Nb-10Zr-5Ta alloy during immersion in simulated physiological solutions: Formation of layers, dissolution and biocompatibility. *J. Mater. Sci. Mater. Med.* **2014**, *25*, 1099–1114. [CrossRef] [PubMed]
98. Nagesh, C.R.V.S.; Ramachandran, C.S.; Subramanyam, R.B. Methods of titanium sponge production. *Trans. Indian Inst. Met.* **2008**, *61*, 341–348. [CrossRef]
99. Subramanyam, R.B. Some recent innovations in the Kroll process of titanium sponge production. *Bull. Mater. Sci.* **1993**, *16*, 433–451. [CrossRef]
100. Fang, Z.Z.; Paramore, J.D.; Sun, P.; Chandran, K.S.R.; Zhang, Y.; Xia, Y.; Cao, F.; Koopman, M.; Free, M. Powder metallurgy of titanium—past, present, and future. *Int. Mater. Rev.* **2017**, 1–53. [CrossRef]
101. Paramore, J.D.; Zak Fang, Z.; Sun, P. 10-Hydrogen sintering of titanium and its alloys. In *Titanium Powder Metallurgy*; Qian, M., Froes, F.H., Eds.; Butterworth-Heinemann: Boston, MA, USA, 2015; pp. 163–182, ISBN 978-0-12-800054-0.
102. Joshi, V.V.; Lavender, C.; Moxon, V.; Duz, V.; Nyberg, E.; Weil, K.S. Development of Ti-6Al-4V and Ti-1Al-8V-5Fe Alloys Using Low-Cost TiH_2 Powder Feedstock. *J. Mater. Eng. Perform.* **2013**, *22*, 995–1003. [CrossRef]
103. Devaraj, A.; Joshi, V.V.; Srivastava, A.; Manandhar, S.; Moxson, V.; Duz, V.A.; Lavender, C. A low-cost hierarchical nanostructured beta-titanium alloy with high strength. *Nat. Commun.* **2016**, *7*, 11176. [CrossRef] [PubMed]
104. Sauer, C.; Luetjering, G. Thermo-mechanical processing of high strength β-titanium alloys and effects on microstructure and properties. *J. Mater. Process Technol.* **2001**, *117*, 311–317. [CrossRef]
105. Jackson, M.; Jones, N.G.; Dye, D.; Dashwood, R.J. Effect of initial microstructure on plastic flow behaviour during isothermal forging of Ti-10V-2Fe-3Al. *Mater. Sci. Eng. A* **2009**, *501*, 248–254. [CrossRef]
106. Boyer, R.R.; Kuhlman, G.W. Processing properties relationships of Ti-10V-2Fe-3Al. *Metall. Trans. A* **1987**, *18*, 2095–2103. [CrossRef]
107. Jones, N.G.; Dashwood, R.J.; Dye, D.; Jackson, M. The Flow Behavior and Microstructural Evolution of Ti-5Al-5Mo-5V-3Cr during Subtransus Isothermal Forging. *Metall. Mater. Trans. A* **2009**, *40*, 1944–1954. [CrossRef]
108. Hua, K.; Xue, X.; Kou, H.; Fan, J.; Tang, B.; Li, J. Characterization of hot deformation microstructure of a near beta titanium alloy Ti-5553. *J. Alloy Compd.* **2014**, *615*, 531–537. [CrossRef]
109. Zhao, J.; Zhong, J.; Chai, F.; Dargusch, M. Deformation behaviour and mechanisms during hot compression at supertransus temperatures in Ti-10V-2Fe-3Al. *J. Alloy Compd.* **2017**, *710*, 616–627. [CrossRef]
110. Lei, L.; Huang, X.; Wang, M.; Wang, L.; Qin, J.; Li, H.; Lu, S. Effect of hot compressive deformation on the martensite transformation of Ti-10V-2Fe-3Al titanium alloy. *Mater. Sci. Eng. A* **2011**, *530*, 591–601. [CrossRef]
111. Warchomicka, F.; Poletti, C.; Stockinger, M. Study of the hot deformation behaviour in Ti-5Al-5Mo-5V-3Cr-1Zr. *Mater. Sci. Eng. A* **2011**, *528*, 8277–8285. [CrossRef]
112. Samiee, A.; Casillas, G.; Ahmed, M.; Savvakin, D.G.; Naseri, R.; Pereloma, E. Formation of Deformation-Induced Products in a Metastable-β Titanium Alloy during High Temperature Compression. *Metals* **2018**, *8*, 100. [CrossRef]
113. Kar, S.K.; Ghosh, A.; Fulzele, N.; Bhattacharjee, A. Quantitative microstructural characterization of a near beta Ti alloy, Ti-5553 under different processing conditions. *Mater. Charact.* **2013**, *81*, 37–48. [CrossRef]
114. Manda, P.; Chakkingal, U.; Singh, A.K. Microstructure, Texture and Mechanical Properties of hot Rolled Metastable β-Titanium Alloy Ti-5Al-5Mo-5V-3Cr. *Mater. Today Proc.* **2015**, *2*, 1118–1126. [CrossRef]

115. Geetha, M.; Singh, A.K.; Gogia, A.K.; Asokamani, R. Effect of thermomechanical processing on evolution of various phases in Ti-Nb-Zr alloys. *J. Alloy Compd.* **2004**, *384*, 131–144. [CrossRef]
116. Lee, T.; Heo, Y.-U.; Lee, C.S. Microstructure tailoring to enhance strength and ductility in Ti-13Nb-13Zr for biomedical applications. *Scr. Mater.* **2013**, *69*, 785–788. [CrossRef]
117. Lee, T.; Park, K.-T.; Lee, D.J.; Jeong, J.; Oh, S.H.; Kim, H.K.; Park, C.H.; Lee, C.S. Microstructural evolution and strain-hardening behavior of multi-pass caliber-rolled Ti-13Nb-13Zr. *Mater. Sci. Eng. A* **2015**, *648*, 359–366. [CrossRef]
118. Lee, W.-S.; Kao, C.-H. Hot deformation behaviour and microstructural evolution of biomedical Ti-13Nb-13Zr alloy in high strain rate range. *Mater. Sci. Eng. A* **2016**, *677*, 230–239. [CrossRef]
119. Bobbili, R.; Madhu, V. Dynamic recrystallization behavior of a biomedical Ti-13Nb-13Zr alloy. *J. Mech. Behav. Biomed. Mater.* **2016**, *59*, 146–155. [CrossRef] [PubMed]
120. Davidson, J.A.; Mishra, A.K.; Kovacs, P.; Poggie, R.A. New surface-hardened, low-modulus, corrosion-resistant Ti-13Nb-13Zr alloy for total hip arthroplasty. *Biomed. Mater. Eng.* **1994**, *4*, 231–243. [PubMed]
121. Karasevskaya, O.P.; Ivasishin, O.M.; Semiatin, S.L.; Matviychuk, Y.V. Deformation behavior of beta-titanium alloys. *Mater. Sci. Eng. A* **2003**, *354*, 121–132. [CrossRef]
122. Dieter, G.E. *Mechanical Metallurgy*, 3rd ed.; McGraw-Hill: Boston, MA, USA, 1986.
123. Campo, K.N.; Andrade, D.R.; Opini, V.C.; Mello, M.G.; Lopes, E.S.N.; Caram, R. On the hardenability of Nb-modified metastable beta Ti-5553 alloy. *J. Alloys Compd.* **2016**, *667*, 211–218. [CrossRef]
124. Santhosh, R.; Geetha, M.; Nageswara Rao, M. Recent Developments in Heat Treatment of Beta Titanium Alloys for Aerospace Applications. *Trans. Indian Inst. Met.* **2017**, *70*, 1681–1688. [CrossRef]
125. Srinivasu, G.; Natraj, Y.; Bhattacharjee, A.; Nandy, T.K.; Nageswara Rao, G.V.S. Tensile and fracture toughness of high strength β Titanium alloy, Ti-10V-2Fe-3Al, as a function of rolling and solution treatment temperatures. *Mater. Des.* **2013**, *47*, 323–330. [CrossRef]
126. Li, C.-L.; Mi, X.-J.; Ye, W.-J.; Hui, S.-X.; Yu, Y.; Wang, W.-Q. Effect of solution temperature on microstructures and tensile properties of high strength Ti-6Cr-5Mo-5V-4Al alloy. *Mater. Sci. Eng. A* **2013**, *578*, 103–109. [CrossRef]
127. Shekhar, S.; Sarkar, R.; Kar, S.K.; Bhattacharjee, A. Effect of solution treatment and aging on microstructure and tensile properties of high strength β titanium alloy, Ti-5Al-5V-5Mo-3Cr. *Mater. Des.* **2015**, *66*, 596–610. [CrossRef]
128. Ivasishin, O.M.; Markovsky, P.E.; Matviychuk, Y.V.; Semiatin, S.L.; Ward, C.H.; Fox, S. A comparative study of the mechanical properties of high-strength β-titanium alloys. *J. Alloy Compd.* **2008**, *457*, 296–309. [CrossRef]
129. Zhang, X.; Kou, H.; Li, J.; Zhang, F.; Zhou, L. Evolution of the secondary α phase morphologies during isothermal heat treatment in Ti-7333 alloy. *J. Alloy Compd.* **2013**, *577*, 516–522. [CrossRef]
130. Ahmed, M.; Li, T.; Casillas, G.; Cairney, J.M.; Wexler, D.; Pereloma, E.V. The evolution of microstructure and mechanical properties of Ti-5Al-5Mo-5V-2Cr-1Fe during ageing. *J. Alloy Compd.* **2015**, *629*, 260–273. [CrossRef]
131. Manda, P.; Singh, V.; Chakkingal, U.; Singh, A.K. Development of α precipitates in metastable Ti-5Al-5Mo-5V-3Cr and similar alloys. *Mater. Charact.* **2016**, *120*, 220–228. [CrossRef]
132. Li, T.; Kent, D.; Sha, G.; Stephenson, L.T.; Ceguerra, A.V.; Ringer, S.P.; Dargusch, M.S.; Cairney, J.M. New insights into the phase transformations to isothermal ω and ω-assisted α in near β-Ti alloys. *Acta Mater.* **2016**, *106*, 353–366. [CrossRef]
133. Li, T.; Kent, D.; Sha, G.; Dargusch, M.; Cairney, J.M. The mechanism of ω-assisted α phase formation in near β-Ti alloys. *Scr. Mater.* **2015**, *104*, 75–78. [CrossRef]
134. Li, T.; Kent, D.; Sha, G.; Cairney, J.M.; Dargusch, M.S. The role of ω in the precipitation of α in near-β Ti alloys. *Scr. Mater.* **2016**, *117*, 92–95. [CrossRef]
135. Zheng, Y.; Williams, R.A.; Sosa, J.M.; Wang, Y.; Banerjee, R.; Fraser, H.L. The role of the ω phase on the non-classical precipitation of the α phase in metastable β-titanium alloys. *Scr. Mater.* **2016**, *111*, 81–84. [CrossRef]
136. Zheng, Y.; Williams, R.E.A.; Wang, D.; Shi, R.; Nag, S.; Kami, P.; Sosa, J.M.; Banerjee, R.; Wang, Y.; Fraser, H.L. Role of ω phase in the formation of extremely refined intragranular α precipitates in metastable β-titanium alloys. *Acta Materialia* **2016**, *103*, 850–858. [CrossRef]

137. Dong, R.; Li, J.; Fan, J.; Kou, H.; Tang, B. Precipitation of α phase and its morphological evolution during continuous heating in a near β titanium alloy Ti-7333. *Mater. Charact.* **2017**, *132*, 199–204. [CrossRef]
138. Devaraj, A.; Williams, R.E.A.; Nag, S.; Srinivasan, R.; Fraser, H.L.; Banerjee, R. Three-dimensional morphology and composition of omega precipitates in a binary titanium-molybdenum alloy. *Scr. Mater.* **2009**, *61*, 701–704. [CrossRef]
139. Devaraj, A.; Nag, S.; Srinivasan, R.; Williams, R.E.A.; Banerjee, S.; Banerjee, R.; Fraser, H.L. Experimental evidence of concurrent compositional and structural instabilities leading to ω precipitation in titanium-molybdenum alloys. *Acta Mater.* **2012**, *60*, 596–609. [CrossRef]
140. Nag, S.; Devaraj, A.; Srinivasan, R.; Williams, R.E.A.; Gupta, N.; Viswanathan, G.B.; Tiley, J.S.; Banerjee, S.; Srinivasan, S.G.; Fraser, H.L.; et al. Novel Mixed-Mode Phase Transition Involving a Composition-Dependent Displacive Component. *Phys. Rev. Lett.* **2011**, *106*, 245701. [CrossRef] [PubMed]
141. Barriobero-Vila, P.; Requena, G.; Warchomicka, F.; Stark, A.; Schell, N.; Buslaps, T. Phase transformation kinetics during continuous heating of a β-quenched Ti-10V-2Fe-3Al alloy. *J. Mater. Sci.* **2015**, *50*, 1412–1416. [CrossRef]
142. Barriobero-Vila, P.; Requena, G.; Schwarz, S.; Warchomicka, F.; Buslaps, T. Influence of phase transformation kinetics on the formation of α in a β-quenched Ti-5Al-5Mo-5V-3Cr-1Zr alloy. *Acta Mater.* **2015**, *95*, 90–101. [CrossRef]
143. Furuhara, T.; Maki, T.; Makino, T. Microstructure control by thermomechanical processing in β-Ti–1513–alloy. *J. Mater. Process. Technol.* **2001**, *117*, 318–323. [CrossRef]
144. Schmidt, P.; El-Chaikh, A.; Christ, H.-J. Effect of Duplex Aging on the Initiation and Propagation of Fatigue Cracks in the Solute-rich Metastable β Titanium Alloy Ti 38-644. *Metall. Mater. Trans. A* **2011**, *42*, 2652–2667. [CrossRef]
145. Santhosh, R.; Geetha, M.; Saxena, V.K.; Nageswararao, M. Studies on single and duplex aging of metastable beta titanium alloy Ti-15V-3Cr-3Al-3Sn. *J. Alloy Compd.* **2014**, *605*, 222–229. [CrossRef]
146. Santhosh, R.; Geetha, M.; Saxena, V.K.; Nageswara Rao, M. Effect of duplex aging on microstructure and mechanical behavior of beta titanium alloy Ti-15V-3Cr-3Al-3Sn under unidirectional and cyclic loading conditions. *Int. J. Fatigue* **2015**, *73*, 88–97. [CrossRef]
147. Coakley, J.; Vorontsov, V.A.; Jones, N.G.; Radecka, A.; Bagot, P.A.J.; Littrell, K.C.; Heenan, R.K.; Hu, F.; Magyar, A.P.; Bell, D.C.; et al. Precipitation processes in the Beta-Titanium alloy Ti-5Al-5Mo-5V-3Cr. *J. Alloys Compd.* **2015**, *646*, 946–953. [CrossRef]
148. Ramesh, A.; Ankem, S. Stress-induced products in a Ti-14.8 V alloy deformed in tension. *Metall. Mater. Trans. A* **1999**, *30*, 2249–2251. [CrossRef]
149. Hanada, S.; Izumi, O. Deformation behaviour of retained β phase inβ-eutectoid Ti-Cr alloys. *J. Mater. Sci.* **1986**, *21*, 4131–4139. [CrossRef]
150. Hanada, S.; Yoshio, T.; Izumi, O. Effect of Plastic Deformation Modes on Tensile Properties of Beta Titanium Alloys. *Trans. JIM* **1986**, *27*, 496–503. [CrossRef]
151. Hanada, S.; Izumi, O. Correlation of tensile properties, deformation modes, and phase stability in commercial β-phase titanium alloys. *Metall. Trans. A* **1987**, *18*, 265–271. [CrossRef]
152. Grosdidier, T.; Combres, Y.; Gautier, E.; Philippe, M.-J. Effect of microstructure variations on the formation of deformation-induced martensite and associated tensile properties in a β metastable Ti alloy. *Metall. Mater. Trans. A* **2000**, *31*, 1095–1106. [CrossRef]
153. Doraiswamy, D.; Ankem, S. The effect of grain size and stability on ambient temperature tensile and creep deformation in metastable beta titanium alloys. *Acta Mater.* **2003**, *51*, 1607–1619. [CrossRef]
154. Wyatt, Z.; Ankem, S. The effect of metastability on room temperature deformation behavior of β and α + β titanium alloys. *J. Mater. Sci.* **2010**, *45*, 5022–5031. [CrossRef]
155. Kim, H.-S.; Lim, S.-H.; Yeo, I.-D.; Kim, W.-Y. Stress-induced martensitic transformation of metastable β-titanium alloy. *Mater. Sci. Eng. A* **2007**, *449–451*, 322–325. [CrossRef]
156. Xu, W.; Kim, K.B.; Das, J.; Calin, M.; Eckert, J. Phase stability and its effect on the deformation behavior of Ti-Nb-Ta-In/Cr β alloys. *Scr. Mater.* **2006**, *54*, 1943–1948. [CrossRef]
157. Bhattacharjee, A.; Bhargava, S.; Varma, V.K.; Kamat, S.V.; Gogia, A.K. Effect of β grain size on stress induced martensitic transformation in β solution treated Ti-10V-2Fe-3Al alloy. *Scr. Mater.* **2005**, *53*, 195–200. [CrossRef]

158. Bhattacharjee, A.; Varma, V.K.; Kamat, S.V.; Gogia, A.K.; Bhargava, S. Influence of β grain size on tensile behavior and ductile fracture toughness of titanium alloy Ti-10V-2Fe-3Al. *Metall. Mater. Trans. A* **2006**, *37*, 1423–1433. [CrossRef]
159. Zhang, L.C.; Zhou, T.; Aindow, M.; Alpay, S.P.; Blackburn, M.J.; Wu, M.H. Nucleation of stress-induced martensites in a Ti/Mo-based alloy. *J. Mater. Sci.* **2005**, *40*, 2833–2836. [CrossRef]
160. Rusakov, G.M.; Litvinov, A.V.; Litvinov, V.S. Deformation twinning of titanium β-alloys of transition class. *Met. Sci. Heat Treat.* **2006**, *48*, 244–251. [CrossRef]
161. Xing, H.; Sun, J. Mechanical twinning and omega transition by ⟨111⟩ {112} shear in a metastable β titanium alloy. *Appl. Phys. Lett.* **2008**, *93*, 031908. [CrossRef]
162. Besse, M.; Castany, P.; Gloriant, T. Mechanisms of deformation in gum metal TNTZ-O and TNTZ titanium alloys: A comparative study on the oxygen influence. *Acta Mater.* **2011**, *59*, 5982–5988. [CrossRef]
163. Ahmed, M.; Wexler, D.; Casillas, G.; Ivasishin, O.M.; Pereloma, E.V. The influence of β phase stability on deformation mode and compressive mechanical properties of Ti-10V-3Fe-3Al alloy. *Acta Mater.* **2015**, *84*, 124–135. [CrossRef]
164. Barriobero-Vila, P.; Gussone, J.; Kelm, K.; Haubrich, J.; Stark, A.; Scheil, N.; Requena, G. An in situ investigation of the deformation mechanisms in a β-quenched Ti-5Al-5V-5Mo-3Cr alloy. *Mater. Sci. Eng. A* **2018**, *717*, 134–143. [CrossRef]
165. Kim, H.Y.; Ikehara, Y.; Kim, J.I.; Hosoda, H.; Miyazaki, S. Martensitic transformation, shape memory effect and superelasticity of Ti-Nb alloys. *Acta Mater.* **2006**, *54*, 2419–2429. [CrossRef]
166. Castany, P.; Ramarolahy, A.; Prima, F.; Lahuerte, P.; Curfs, C.; Gloriant, T. In situ synchrotron X-ray diffraction study of the martensitic transformation in superelastic Ti-24Nb-0.5N and Ti-024Nb-0.5O alloys. *Acta Mater.* **2015**, *88*, 102–111. [CrossRef]
167. Ijaz, M.F.; Kim, H.Y.; Hosoda, H.; Miyazaki, S. Effect of Sn addition on stress hysteresis and superelastic properties of a Ti-15Nb-3Mo alloy. *Scr. Mater.* **2014**, *72–73*, 29–32. [CrossRef]
168. López Pavón, L.; Kim, H.Y.; Hosoda, H.; Miyazaki, S. Effect of Nb content and heat treatment temperature on superelsatic properties of Ti-24Zr-(8–12)Nb-2Sn alloys. *Scr. Mater.* **2015**, *95*, 46–49. [CrossRef]
169. Ijaz, M.F.; Kim, H.Y.; Hosoda, H.; Miyazaki, S. Superelastic properties of biomedical (Ti-Zr)-Mo-Sn alloys. *Mater. Sci. Eng. A.* **2015**, *48*, 11–20. [CrossRef] [PubMed]
170. Fu, J.; Yamamoto, A.; Kim, H.Y.; Hosoda, H.; Miyazaki, S. NOvel Ti-base superelastic alloys with large recovery strain and excellent biocompatibility. *Acta Biomater.* **2015**, *17*, 56–67. [CrossRef] [PubMed]
171. Fu, J.; Kim, H.Y.; Miyazaki, S. Effect of annealing temperature on microstructure and superelastic properties of a Ti-18Zr-4.5Nb-3Sn-2Mo alloy. *J. Mech. Behav. Biomed. Mater.* **2017**, *65*, 716–723. [CrossRef] [PubMed]
172. Yang, Y.; Castany, P.; Cornen, M.; Thibon, I.; Prima, F.; Gloriant, T. Texture investigation of the superelastic Ti-24Nb-4Zr-8Sn alloy. *J. Alloy Compd.* **2014**, *591*, 85–90. [CrossRef]
173. Yang, Y.; Castany, P.; Cornen, M.; Prima, F.; Li, S.J.; Hao, Y.L.; Gloriant, T. Characterization of the martensitic transformation in the superelastic Ti-24Nb-4Zr-8Sn alloy by in situ synchrotron X-ray diffraction and dynamic mechanical analysis. *Acta Mater.* **2015**, *88*, 25–33. [CrossRef]
174. Herzog, D.; Seyda, V.; Wysick, E.; Emmelmann, C. Additive manufacturing of metals. *Acta Mater.* **2016**, *117*, 371–392. [CrossRef]
175. Hernandez, J.; Li, S.J.; Martinez, E.; Murr, L.E.; Pan, X.M.; Amato, K.N.; Cheng, X.Y.; Yang, F.; Terrazas, C.A.; Gayton, S.M.; et al. Microstructures and Hardness Properties for β-Phase Ti-24Nb-4Zr-7.9 Sn Alloy Fabricated by Electron Beam Melting. *J. Mater. Sci. Technol.* **2013**, *29*, 1011–1017. [CrossRef]
176. Liu, Y.; Li, S.; Hou, W.; Wang, S.; Hao, Y.; Yang, R.; Sercombe, T.B.; Zhang, L.-C. Electron Beam Melted Beta-type Ti-24Nb-4Zr-8Sn Porous Structures with High Strength-to-Modulus Ratio. *J. Mater. Sci. Technol.* **2016**, *32*, 505–508. [CrossRef]
177. Liu, Y.J.; Li, S.J.; Wang, H.L.; Hou, W.T.; Hao, Y.L.; Yang, R.; Sercombe, T.B.; Zhang, L.C. Microstructure, defects, and mechanical behavior of beta-type titanium porous structures manufactured by electron beam melting and selective laser melting. *Acta Mater.* **2016**, *113*, 56–67. [CrossRef]
178. Liu, Y.J.; Wang, H.L.; Li, S.J.; Wang, S.G.; Wang, W.J.; Hou, W.T.; Hao, Y.L.; Yang, R.; Zhang, L.C. Compressive and fatigue behavior of beta-type titanium porous structures fabricated by electron beam melting. *Acta Mater.* **2017**, *126*, 58–66. [CrossRef]
179. Zhang, L.C.; Klemm, D.; Eckert, J.; Hao, Y.L.; Sercombe, T.B. Manufacture by selective laser melting and mechanical behavior of a biomedical Ti–24Nb–4Zr–8Sn alloy. *Scr. Mater.* **2011**, *65*, 21–24. [CrossRef]

180. Liu, Y.J.; Li, X.P.; Zhang, L.C.; Sercombe, T.B. Processing and properties of topologically optimised biomedical Ti-24Nb-4Zr-8Sn scaffolds manufactured by selective laser melting. *Mater. Sci. Eng. A.* **2015**, *642*, 268–278. [CrossRef]
181. Wang, Q.; Han, C.; Choma, T.; Wei, Q.; Yan, C.; Song, B.; Shi, Y. Effect of Nb content on microstructure, property and in vitro apatite-forming capability of Ti-Nb alloys fabricated via selective laser melting. *Mater. Des.* **2017**, *126*, 268–277. [CrossRef]
182. Ishimoto, T.; Hagihara, K.; Hisamoto, K.; Sun, S.-H.; Nakano, T. Crystallographic texture control of beta-type Ti–15Mo–5Zr–3Al alloy by selective laser melting for the development of novel implants with a biocompatible low Young's modulus. *Scr. Mater.* **2017**, *132*, 34–38. [CrossRef]
183. Devaraj, A.; Perea, D.E.; Liu, J.; Gordon, L.M.; Prose, T.J.; Parikh, P.; Diercks, D.R.; Meher, S.; Kolli, R.P.; Meng, Y.S.; et al. Three-dimensional nanoscale characterisiation of materials by atom probe tomography. *Int. Mater. Rev.* **2018**, *63*, 68–101. [CrossRef]
184. Kolli, R.P. Atom Probe Tomography: A Review of Correlative Analysis of Interfaces and Precipitates in Metals and Alloys. *JOM* **2018**, in press. [CrossRef]